Available online at www.sciencedirect.com

ScienceDirect

J Materiomics 1 (2015) 263–284

www.ceramsoc.com/en/

www.journals.elsevier.com/journal-of-materiomics/

Multiferroic heterostructures and tunneling junctions

Weichuan Huang [a], Shengwei Yang [a], Xiaoguang Li [a,b,c,*]

[a] Hefei National Laboratory for Physical Sciences at Microscale, Department of Physics, University of Science and Technology of China, Hefei 230026, China
[b] Collaborative Innovation Center of Advanced Microstructures, Nanjing University, Nanjing 210093, China
[c] Key Laboratory of Materials Physics, Institute of Solid State Physics, CAS, Hefei 230031, China

Received 18 June 2015; revised 22 July 2015; accepted 14 August 2015
Available online 24 August 2015

Abstract

Multiferroic heterostructures showing both electric and magnetic orders have attracted much attention because of their promising applications in the next generation of memories, sensors, and microwave devices and so on. The complex electronic and magnetic orders at the interface in multiferroic heterostructures will cause abundant physical phenomena due to the interplay among spin, charge, orbit, and lattice degrees of freedom, and various prototype devices have been achieved. In this review, we summarize some recent progresses mainly in the strain- and charge-mediated effects on the magnetic and electronic transport properties manipulated by electric/magnetic fields in multiferroic heterostructures. The recent advances in multiferroic tunnel junctions with ferroelectric barriers by using the spin polarized nature of magnetic materials are particularly presented, which exhibit magnetoelectric coupling effects at the interface and multi-stable resistance states in a single memory unit cell. Finally, the new inspiration for the design of spintronic devices having more energy efficiency and higher density is discussed.

Keywords: Multiferroic heterostructure; Multiferroic tunnel junctions; Magnetoelectric coupling; Strain and charge effects

1. Introduction

Multiferroic materials [1,2], which simultaneously show at least two ferroic orderings, such as ferroelectric and (anti-) ferromagnetic as well as ferroelectric, have recently become one of the hottest topics in condensed matter physics and materials due to their novel physical phenomena and potential applications as multifunctional devices such as spintronics and multiple-state memories [3–10]. Among multiferroic orderings, the coexistence of ferroelectricity and ferromagnetism is highly desired, and the coupling between the two different orders can produce the magnetoelectric (ME) effect which has been observed as an intrinsic effect in some natural single phase materials [11], such as $BiFeO_3$ (BFO), one of the most intensively investigated single phase multiferroics [12]. Despite the ongoing search for new intrinsic single phase multiferroic compounds, there still exist so many questions, for instance, ME coupling interactions i) are very weak for type I single phase multiferroic materials in which the ferroelectric and magnetic order are produced by different sublattices or parts of the lattice [13–15], and ii) mostly exist at low temperatures with a small value of polarization for type II single phase multiferroics oxides where the ferroelectricity is magnetically induced [15,16]. Up to now, none of the existing single phase multiferroic materials has large, robust electric and magnetic polarizations at room temperature.

Fortunately, a significant ME coupling effect can be achieved in multiferroic composites consisting of ferroelectric and ferromagnetic phases through manipulating magnetization rotation by electric control at room temperature [17–22]. The multiferroic ME composites constructed as nanostructures (*e.g.*, 0–3 type particulate films, 2-2 type layered heterostructures, and 1–3 type vertical heterostructures) [17],

* Corresponding author. Hefei National Laboratory for Physical Sciences at Microscale, Department of Physics, University of Science and Technology of China, Hefei 230026, China.
E-mail address: lixg@ustc.edu.cn (X. Li).
Peer review under responsibility of The Chinese Ceramic Society.

http://dx.doi.org/10.1016/j.jmat.2015.08.002

especially multiferroic heterostructures, have unique superiorities. More significant ME coupling can be realized and effectively manipulated in limited heterostructure regions at room temperature. More importantly, from the application viewpoint, multiferroic heterostructures are promising candidates for integrated magnetic/electric devices, such as highly sensitive sensors, high-density memories, and spintronics, and are easier to be fabricated by utilizing wide variety of growth techniques, such as pulsed laser deposition, molecular beam epitaxy, magnetron sputtering, spin coating and so on.

In this article, we review some recent progresses mainly in electric-field manipulated magnetic and electronic transport properties in virtue of strain- and charge-mediated ME effects. The Secs. 2 and 3 focus on the ferromagnetic/ferroelectric (FM/FE) multiferroic heterostructures and multiferroic tunnel junctions (MFTJs), respectively, which have recently attracted much attention as new concepts for information processing and storage due to multi-states in a single memory unit cell. Finally, in Sec. 4 the summary and outlook are given. Since the research area is broad and rapidly developing, the extensively amount of research on various multiferroic heterostructures have been published every year, so we apologize to the authors of these in advance which have unfortunately not been cited.

2. Multiferroic heterostructure

2.1. Strain-mediated ME coupling

The ME coupling effects can be divided mainly into two categories: magnetic field (H) control of electric polarization (direct ME coupling) [23–27] and electric field (E) control of magnetism (converse ME coupling) [28–31]. The ME couplings in multiferroic composites are generally caused through the interaction between electric and magnetic orders from two distinct phases. A magnetic or electric field induces strain in the magnetic or ferroelectric constituent which is mechanically transferred to the ferroelectric or magnetic constituent, and it will result in a variation of ferroelectric polarization or magnetization. Thus, in order to obtain a significant ME coupling, it is necessary to employ ferroelectric materials with large piezoelectric coefficients, magnetic materials with large magnetostriction coefficients, and strong mechanical contacts between the different phases in multiferroic heterostructures.

To reveal the magnetic field control of electric polarization, T. Wu et al. investigated an epitaxial piezoelectric $Pb(Zr_{0.3},Ti_{0.7})O_3$ film grown on the magnetostrictive single crystal $La_{1.2}Sr_{1.8}Mn_2O_7$, where a strong mechanical coupling at the interface helped to achieve a considerable ME response [27]. They obtained a maximum ME voltage output of ΔV_{ME} ~15 μV at 120 K in a magnetic field of 1 T as shown in Fig. 1, and the ME coefficient is about 600 mV $cm^{-1}\cdot Oe^{-1}$. Such a magnetic-field-induced ME coupling effect of the ME composite thin films has potential applications as microsensors [32]. While for the electric field control of magnetism it becomes a hot issue in the fields of ME heterostructures recently due to their novel potential applications which have also been

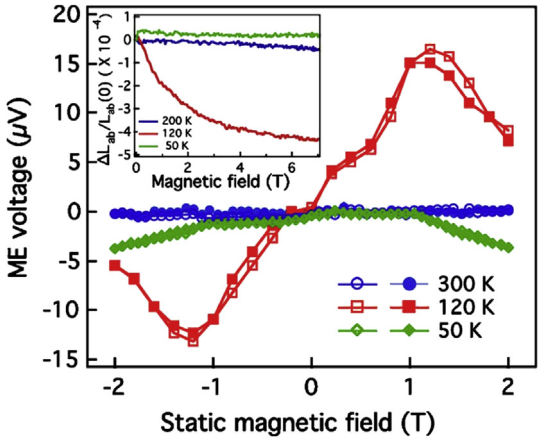

Fig. 1. ME voltage *vs.* static magnetic field measured at temperatures of 50, 120, and 300 K in $Pb(Zr_{0.3},Ti_{0.7})O_3$//$La_{1.2}Sr_{1.8}Mn_2O_7$ multiferroic heterostructure. The open (filled) symbols are the data taken with increasing (decreasing) H. Reprinted by permission from Ref. [27]. The inset is the in-plane magnetostriction $[\Delta L_{ab}(H)/L_{ab}(0)]$ as a function of H measured at selected temperatures, taken from earlier report [34].

reviewed in Ref. [32]. It is reported that, in the heterostructure of 100 nm thick Ni film grown on $BaTiO_3$ (BTO) single crystal substrate, the reversible changes of magnetization (M) up to 20% were observed as a function of electric fields with butterfly-like ME loops under a constant magnetic field parallel to the Ni film plane, as shown in Fig. 2 [33]. This implies that the strain induced by an electric field in BTO is transferred into the ferromagnetic Ni layer, it then affect the magnetization of Ni due to the inverse magnetostriction.

To improve the ME effect, one may select materials with larger piezoelectric coefficients such as $Pb(Mg_{1/3}Nb_{2/3})O_3$-$PbTiO_3$ (PMN-PT). Y. G. Zhao et al. reported a giant volatile electrical manipulation of magnetization at room temperature in a heterostructure composed of amorphous ferromagnetic $Co_{40}Fe_{40}B_{20}$ and (011)-cut PMN-PT as shown in Fig. 3(a) [30]. A maximum relative magnetization change up to 83% was observed. The (011)-cut PMN-PT has the optimized

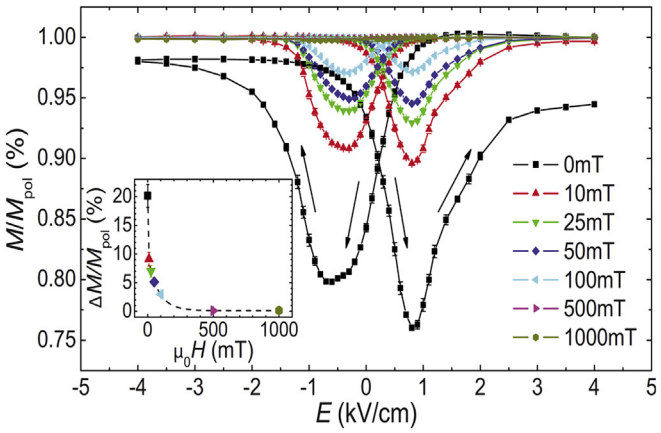

Fig. 2. Magnetization of a 100 nm thick Ni film on BTO *vs.* the electric field applied across the BTO substrate at different magnetic fields. Magnetization is normalized to the value M_{pol} obtained at $E = +4$ kV/cm. Reprinted by permission from Ref. [33].

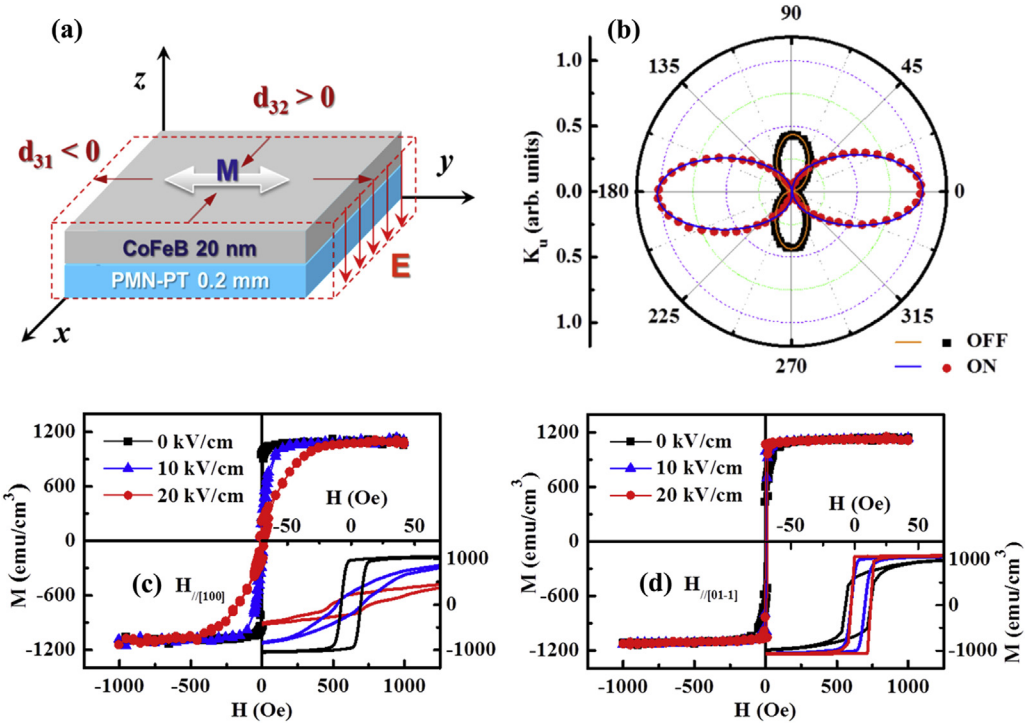

Fig. 3. (a) Schematic illustration of the heterostructure, piezoresponse of the PMN-PT substrate and the easy axis of magnetization of the $Co_{40}Fe_{40}B_{20}$ layer under electric fields. (b) Polar graph of uniaxial anisotropy energy with $E = 17.5$ kV/cm on (red circle) and off (black square). (c) and (d) Magnetic hysteresis loops measured along the [100] and [01$\bar{1}$] directions at different electric fields, respectively. Insets of (c) and (d) show the expanded region of *M-H* at low magnetic fields. Reprinted by permission from Ref. [30].

orientation and composition to achieve ultra-high in-plane piezoelectric coefficients with $d_{31} \sim -3100$ pC/N along the [100] direction and d_{32}~1400 pC/N along the [01$\bar{1}$] direction [35], respectively. The results of Magnetic Optic Kerr Effect with a rotating field (Rot-MOKE) measurement shown in Fig. 3(b) demonstrate a 90° rotation of the easy axis above 5 kV/cm due to the electric field induced in-plane strain anisotropy related to ferroelectric polarization reorientation. When electric fields increase from 0 kV/cm to 20 kV/cm, the magnetization orientation of the heterostructure along the [100] direction becomes harder and the remnant magnetization reduces, as shown in Fig. 3(c). However, the situation along the [01$\bar{1}$] direction is just the converse, with an increment of the *M-H* squareness under large electric fields as shown in Fig. 3(d). These results can be understood by the anisotropic strain of the (011)-cut PMN-PT under electric fields as mentioned above, which generates an in-plane magnetically anisotropic field in $Co_{40}Fe_{40}B_{20}$ film and achieves a 90° rotation of the easy axis as well as a large magnetization response to electric fields [30]. Furthermore, with the assistance of a weak magnetic field (±5 Oe), a reversible and deterministic magnetization reversal controlled by pulsed electric fields has been achieved.

However, the volatile magnetization variations induced by a strain effect mentioned above cannot be used for information storage. Thus researchers start to peruse the electric controlled nonvolatile magnetization variations. Fortunately, a possibility of inducing 90° magnetization rotation controlled by electric fields in arrays of strain coupled artificial Ni/PMN-PT(011) multiferroic nanostructures was demonstrated by using X-ray photoemission electron microscopy (X-PEEM) as shown in Fig. 4 [36]. Fig. 4(b) depicts the in-plane anisotropic strain provided by PMN-PT(011) with a peak at the coercive field (E_c) of 0.15 MV/m. The X-PEEM results are shown in Fig. 4(c). (i) For the ellipses circled in blue, the magnetic contrasts in the nanoislands drop from the original value to zero at E_c, indicating that the magnetizations of the ellipses have rotated away from the long axis and lie parallel to the ellipse short axis. By increasing the electric field up to 0.27 MV/m, no obvious changes in the magnetic configuration are observed. (ii) The ellipses with green triangles show a different behavior. After the 90° reorientation at E_c, the magnetizations relax back to one of the two equivalent directions parallel to the shape anisotropy easy axis after the applied electric field further increased. (iii) The ellipses highlighted with orange squares do not show any change under different applied electric fields. The 90° reorientation results from the strain-induced ME interaction between the ferromagnetic nanostructures and the ferroelectric crystal. The above three strain-induced regimes of magnetization behaviors are regarded to be related to the different ferroelectric domain structures which can be changed by applied electric fields. Interestingly, N. D. Mathur et al. have experimentally demonstrated a nonvolatile electrically driven repeatable out-of-plane magnetization reversal in Ni/BTO multilayer capacitors without magnetic fields [37]. A peak-to-peak phase shift

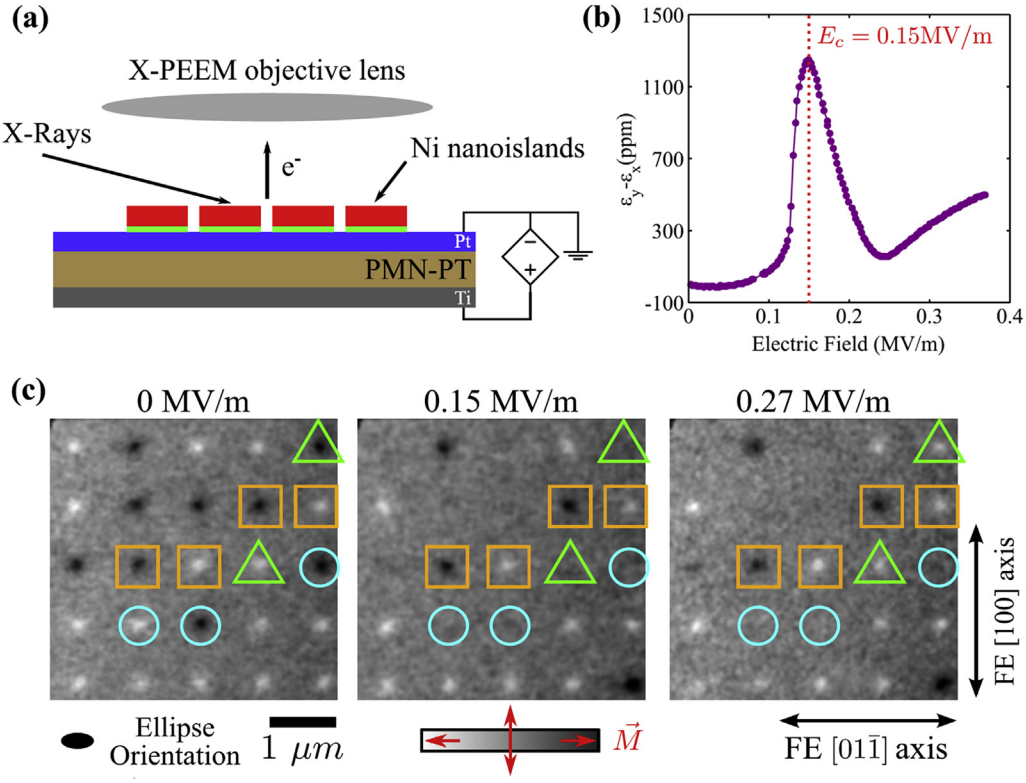

Fig. 4. (a) Schematic of the experiments (not to scale). (b) In-plane anisotropic strain *vs*. electric field curve measured with a strain gauge fixed on the sample after poling. (c) Sequence of successive X-ray magnetic circular dichroism images of 200 × 100 nm^2 ellipse array recorded at the Ni L_3 edge at different electric fields. Reprinted by permission from Ref. [36].

of ~4° corresponding to the full (180°) magnetization reversal was observed in magnetic force microscope by applying and subsequently removing voltages to the multilayer capacitors. These applied voltages also resulted in various ME responses with volatile, non-volatile, repeatable, or non-repeatable effect, similar to those shown in Fig. 4 [36].

However, it is still the most pressing needs to achieve a uniform, reversible and nonvolatile magnetization rotation in large area of a heterostructure via a convenient method. Note that the previously reported electrical manipulation for magnetization reorientation employs a traditional out-of-plane polarization configuration [38–40], in which a magnetic layer also serves as a polarization electrode. In such a structural configuration, the piezoelectric and ferroelectric field effects coexist, and the electric field effect will somehow impact the magnetism and inevitably complicate the physical processes [40]. Taking these problems into account, a promising side-polarization configuration is proposed to separate the polarization electrode and the magnetic layer, which effectively rules out the impact of ferroelectric field effect, and enables a purely piezostrain-mediated ME coupling [41]. In addition, this configuration can directly offer more impressive tensile strain owe to a much larger d_{33} than d_{31} in PMN-PT(001) [42,43].

In our recent work, a strain-mediated reversible and nonvolatile 90° rotation of the magnetic easy axis (MEA) was realized in a Co/PMN-PT heterostructure [41]. In order to investigate the magnetic anisotropy manipulated by an *in-situ* piezostrain, the detailed polarization history dependencies of MEA demonstrated by angle dependencies of the remnant magnetization ratio are shown in Fig. 5 via Rot-MOKE method [44]. Fig. 5(a) indicates an asymmetric butterfly-like piezostrain-electric field loop for the PMN-PT. Several representative electric fields labeled with different colorized symbols on the loop are chosen to clarify the rotation process of MEA. The PMN-PT has been initially negatively polarized. The MEA locates at 0°, namely along [010]/[0$\bar{1}$0] of PMN-PT, for the electric fields starting from $E = 0$ kV/cm [red line in Fig. 5(b)] to 1.5 kV/cm [Fig. 5(c)], changes to 30° at 3.5 kV/cm [Fig. 5(d)], and finally rotates to 90°, namely along [100]/[$\bar{1}$00], at 5 kV/cm [cyan line in Fig. 5(e)], demonstrating an anticlockwise gradual rotation of MEA with increasing electric fields in positive polarizations. Then the MEA keeps stable even after electric field falls back to 0 kV/cm [magenta line in Fig. 5(e)], indicating a nonvolatile tuning of MEA. When the electric field reverses to $E = -1$ kV/cm [Fig. 5(f)], the MEA rapidly turns back to 0° from 90°. During the negative polarization processes, the MEA gradually switches from 0° at $E = -2$ kV/cm [Fig. 5(g)] to −40° at $E = -8$ kV/cm [Fig. 5(i)] and then goes back to 0° again [olive line in Fig. 5(b)]. The MEA-rotation processes can be well repeated at 10 different random spots on the Co film at least. The 90°-rotation of MEA comes from the competition between the magnetoelastic anisotropy induced by the strain transferred

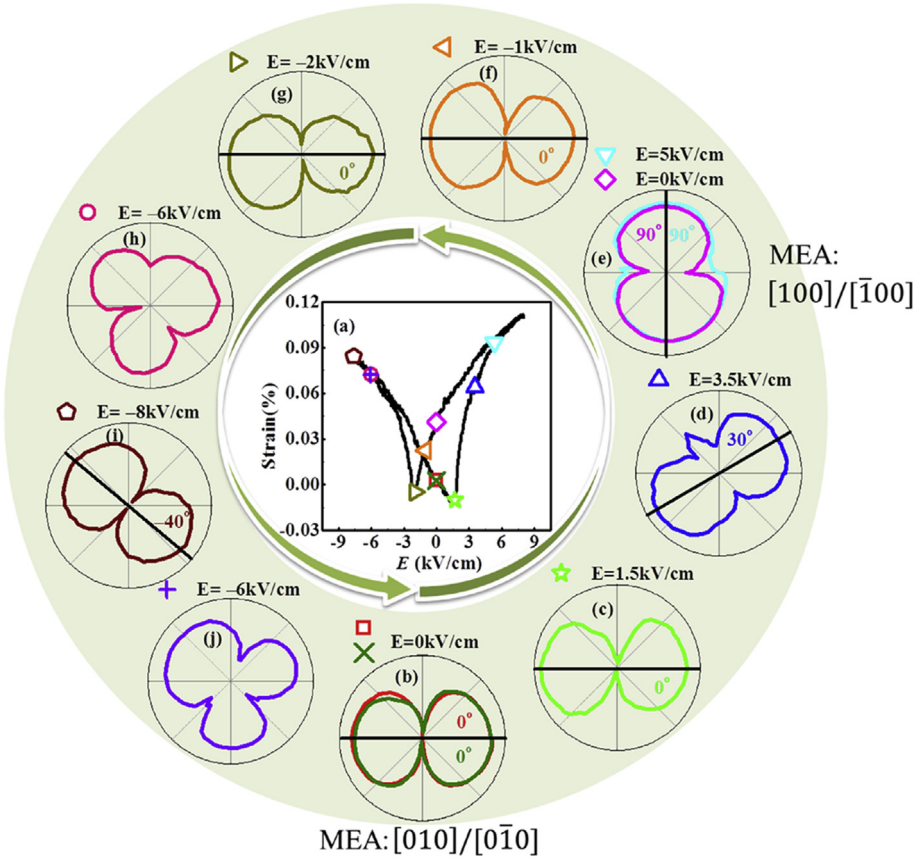

Fig. 5. (a) In-plane strain (ε_{11}) – electric field loop along the [100] direction of PMN-PT. (b–j) Rotation history of the MEA in the Co film with a sequence of electric fields (labeled by corresponding symbols on the strain curve) applied to PMN-PT along the [100] direction in the order from (b) to (j). In (e), after a field of 5 kV/cm is switched off, the MEA does not go back to 0° but remains at 90°. Reprinted by permission from Ref. [41].

from polarized PMN-PT and the interface anisotropy. The asymmetric piezostrain-electric field loop accompanied with a considerable residual strain at 0 kV/cm may be resulted from the field induced phase transition in PMN-PT.

Further experimental results indicate there is a macroscopically maneuverable and non-volatile 180° magnetization reversal without applied magnetic fields at room temperature [41]. The magnetization measurements using superconducting quantum interference device-vibrating sample magnetometer to demonstrate a 180° magnetic rotation under periodic stimuli sequences of ±5 kV/cm, as shown in Fig. 6(a and b). It is clearly revealed that the magnetization switches by 180° from stage 1 (M//[010]) to stage 3 (M//[0$\bar{1}$0]) via stage 2 (M//[$\bar{1}$00]) with first +5 kV/cm followed with −5 kV/cm, and then goes back to stage 1 (M//[010]) via stage 4 (M//[$\bar{1}$00]) under a stimuli sequence of +5 kV/cm and −5 kV/cm together with a very small auxiliary magnetic field H_{au} of 5 Oe. This electric-field-driven reversible 180° rotation occurs in most of the magnetic domains, which is much more than those in earlier reports. It should be noted that corresponding to the non-volatile 90°-rotation of MEA in Co film, a non-volatile anisotropic resistivity switch also occurs [45].

The discovery of electric field-induced non-volatile, repeatable magnetization rotation accompanied by the variation of anisotropic resistivity can be utilized to design electromagnetic devices, such as a digital single-pole double-throw switch and a three-state output gate as well as a spin valve controlled by electric fields instead of magnetic fields [41,45]. N. Lei et al. reported that magnetic coercivity could also be electrically controlled at room temperature via strain-mediated ME coupling in piezoelectric/ferromagnetic

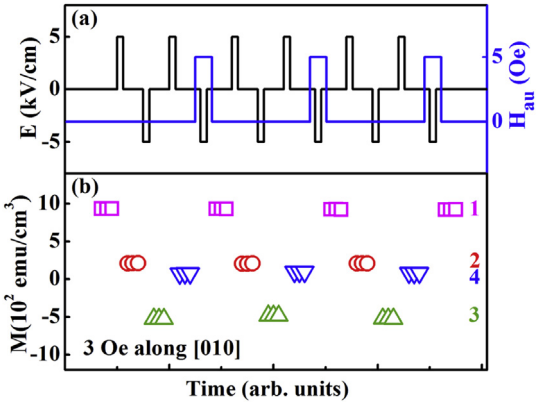

Fig. 6. (a) Pulsed electrical operation (black line) with H_{au} (blue line), and (b) the corresponding magnetic moments measured in a magnetic field of 3 Oe along [010]. The colorful numbers denote the stages 1–4. Reprinted by permission from Ref. [41].

nanostructures with a similar side-polarization configuration [46]. The side-polarization device geometry allows for an efficient transfer of a strong local strain to the ferromagnetic stripe as shown in Fig. 7(a and b). The ferromagnetic spin valves consisting of MgO (2 nm)/free layer/Cu (4 nm)/Co (4 nm)/Cu (0.3 nm)/IrMn (8 nm)/Pt (4 nm), where the free layer was either $Co_{40}Fe_{40}B_{20}$ (5 nm) or permalloy (5 nm)/$Co_{40}Fe_{40}B_{20}$ (5 nm), were constructed, in conjunction with the piezoelectric material $PbZr_{0.5}Ti_{0.5}O_3$. Fig. 7(c) shows a large increase of the magnetic coercivity of the free layer under piezostrain induced by the applied voltage across $PbZr_{0.5}Ti_{0.5}O_3$, which would affect the magnetization reversal in free layer.

Magnetic variations driven by electric fields occur not only in ferromagnetic (FM) films but also in anti-ferromagnetic (AFM) materials. In FeRh/BTO heterostructure a moderate electric field can produce a giant magnetization variation, arising from the electric-field-induced transformation of FeRh from an AFM state to a FM state as shown in Fig. 8 [47]. The effect occurs just above room temperature and is mostly driven by voltage-induced strain effect from BTO. The charge accumulation and depletion effects related to the ferroelectric polarization of BTO may contribute the magnetic variations as well. Fig. 8(a) shows a typical ferroelectric loop for an FeRh/BTO sample, measured at 300 Hz and room temperature. To probe the influence of ferroelectricity on the magnetic response of FeRh, the temperature dependent magnetization measurements were performed with different applied voltages

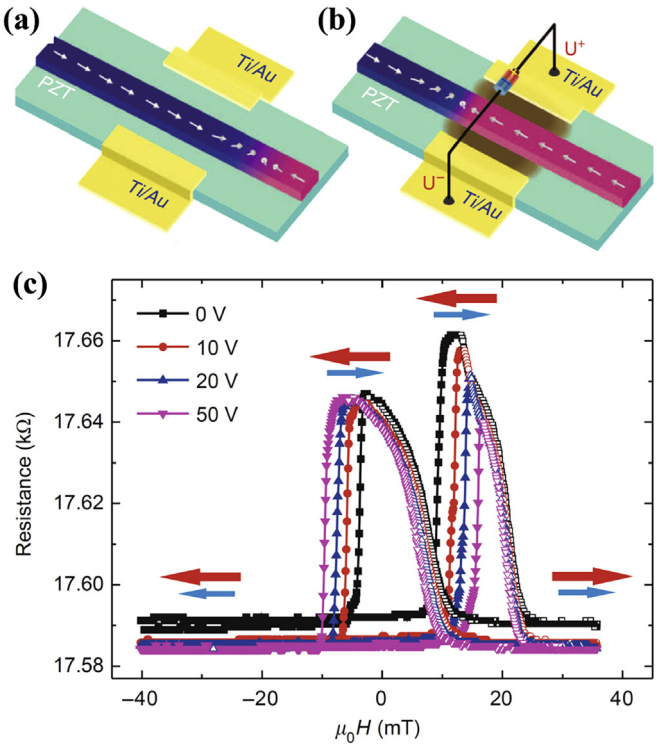

Fig. 7. As-grown magnetization configurations in the magnetic stripe (a) without and (b) with applied voltages. (c) Giant magnetoresistance loops with different applied voltages, starting from a depolarized state of the $PbZr_{0.5}Ti_{0.5}O_3$ layer. Reprinted by permission from Ref. [46].

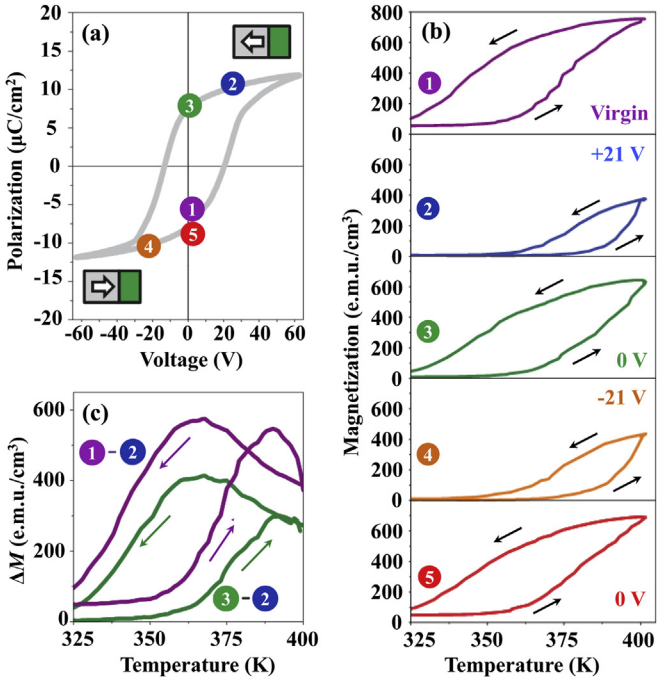

Fig. 8. Influence of applied voltages on the temperature dependences of magnetizations in FeRh/BTO. (a) Polarization *vs.* voltage loop collected at 300 Hz and room temperature. The sketches indicate the polarization of the BTO pointing towards or away from FeRh (green rectangle), at negative or positive voltage, respectively. (b) Temperature dependences of magnetizations measured at 20 kOe for various voltages. (c) Differences of the magnetizations between selected curves from (b). Reprinted by permission from Ref. [47].

marked by numbers in a magnetic field of 20 kOe. The significant magnetization enhancement with increasing temperature in Fig. 8(b) represents the transition of FeRh from an AFM state to a FM state, accompanied with thermal hysteresis resulting from substrate-induced strain. For temperatures between ~350 and 400 K, the magnetization is drastically changed by the applied voltage, with maximum variation reaching $\Delta M = 550$ emu cm^{-3} at electric fields of $E = 0.4$ kV/cm in Fig. 8(c). This corresponds to a gigantic ME coupling $\alpha = \mu_0 \Delta M/E = \mu_0$ (550 emu cm^{-3})/(0.4 kV cm^{-1}) = 17 Oe cm V^{-1}. It would be much more useful that the AFM-FM transition can be achieved at room temperature via electric field manipulation.

2.2. Charge-mediated ME coupling

Other than the strain effect that can be active in relatively thick magnetic films of multiferroic heterostructures, the charge effect is limited to a small screening length of magnetic film, especially the magnetic metallic films with high carrier density. M. Liu et al. have demonstrated the reversible and non-volatile magnetization variations by charge-mediated ME coupling through applying an electric voltage of 10 V in $Co_{0.3}Fe_{0.7}/Ba_{0.6}Sr_{0.4}TiO_3$/Nb:$SrTiO_3$ (001) multiferroic heterostructure [48]. The charge effect can exist only in ultra-thin (~1 nm) magnetic films due to the Thomas-Fermi screening effect. As the thickness of magnetic metallic film increases to >>1 nm, the charge effect disappears rapidly [40,49,50].

In order to investigate the effect of electric fields on magnetic properties of magnetic films with different thicknesses in detail, the multiferroic heterostructure consisting of a magnetic film with continuously varied thickness is constructed as shown in Fig. 9 [51]. The schematic side view of the sample is depicted in Fig. 9(a). The electric polarization state of a polymer ferroelectric thin film substantially alters the magnetic anisotropy of a wedge-shaped Co film with varying thickness under P(VDF-TrFE), indicating the changes of the magnetization easy axis from out-of-plane to in-plane for sufficiently thin ferromagnetic films. The Co strip is 40 mm long with a very shallow wedge angle of 2.7×10^{-6} deg. The anisotropy of the wedge-shaped magnetic film goes from out-of-plane at the thinnest end to in-plane at the thickest end, undergoing a well-known spin reorientation transition at an intermediate thickness. The ME effect shown in Fig. 9(b) indicates that the out-of-plane magnetic coercivity measured by MOKE for the up polarization is larger than that for the down polarization. The effective uniaxial anisotropy constants K_{eff} for both polarization directions were calculated in Fig. 9(c), and a positive value of K_{eff} corresponds to out-of-plane anisotropy. For the smallest Co thickness, switching the ferroelectric polarization to the down state (positive interface charge) alters the uniaxial anisotropy from positive to negative, allowing for electric field controlled switching of the magnetization easy axis from out-of-plane to in-plane. The investigations of the magnetic coercivity at intermediate polarization states demonstrated that the magnetic coercive field was proportional to the net ferroelectric polarization, as shown in Fig. 9(d). This results indicate the central role of the switchable polarization of the ferroelectric film, *i.e.*, charge effect, in the ME coupling.

As for the multiferroic heterostructures consisting of doped manganite layers in contact with the ferroelectric materials, the interfacial charge effect would induce magnetic reconstructions driven by screening effect. D. Yi et al. reported the ability to manipulate the competition between FM and AFM through ME coupling at the BFO/$La_{0.5}Ca_{0.5}MnO_3$ heterointerface [52]. The magnitudes of magnetizations in both interfacial BFO and $La_{0.5}Ca_{0.5}MnO_3$ change dramatically in response to the ferroelectric polarization switch, which is clarified by using a macroscopic magnetometry and element-selective X-ray magnetic circular dichroism (XMCD) at the Mn and Fe *L* edges. In Fig. 10(c), the black (line with solid square), red (line with solid circle), and blue (line with half-filled diamond) curves show the magnetizations of the H1 heterostructure on $SrTiO_3$ (STO) substrate in Fig. 10(a) for the as-grown state (P1, denotes the polarization points away from the interface), the opposite state (P2, denotes the polarization towards the interface) switched by positive voltage, and the original state (P1) switched back by negative voltage. The saturation-like behavior between 100 K and 200 K suggests

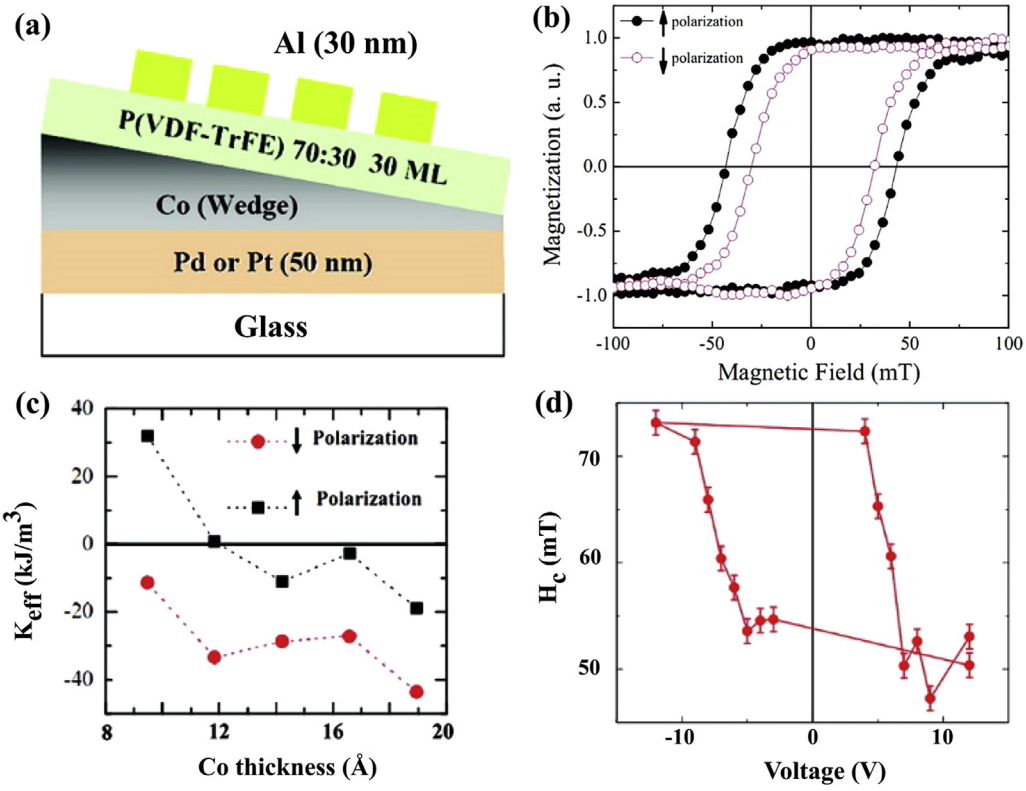

Fig. 9. (a) Schematic side view of the sample: glass/(Pd or Pt)/Co (8.5–27.8 Å)/30 monolayers P(VDF-TrFE) 70:30/Al (30 nm). (b) Out-of-plane magnetic hysteresis loops at a Co thickness of 9.5 Å using polar magneto-optical Kerr effect (PMOKE) depicting the change in coercivity for two different polarization states. (c) Effective uniaxial anisotropy constants as a function of Co thickness for samples on a Pd seed layer for two opposite polarization directions. (d) Out-of-plane magnetic coercivity as a function of applied voltage. Reprinted by permission from Ref. [51].

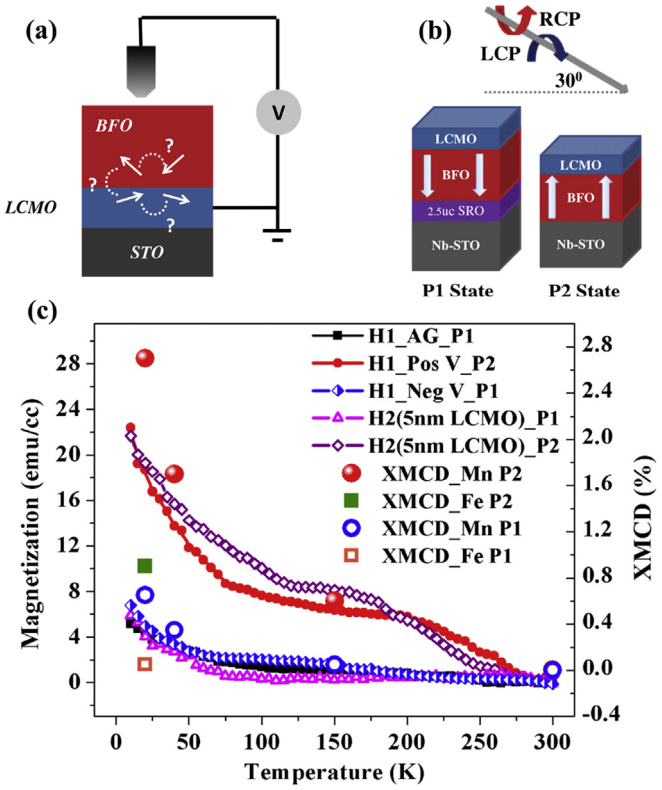

Fig. 10. (a) Schematic of the BFO/$La_{0.5}Ca_{0.5}MnO_3$ (structure H1) heterostructures on STO substrates for ferroelectric switching. (b) Schematic of $La_{0.5}Ca_{0.5}MnO_3$/BFO (structure H2) heterostructure used for XMCD measurements. (c) Temperature dependences of magnetizations and the spin sum rule of XMCD for Fe and Mn atoms taken at different polarization states. Reprinted from Ref. [52].

FM clusters or canted AFM ordering [53,54]. These data clearly show that the AFM-FM transition can be reversibly manipulated through ferroelectric switching. In order to identify the contribution from $La_{0.5}Ca_{0.5}MnO_3$ and BFO, respectively, the element-specific XMCD was further utilized to detect a reversed H2 heterostructure in Fig. 10(b). The significant changes in both Fe and Mn *L* edges, as summarized in Fig. 10(c), illustrate that the ferroelectric polarization manipulated magnetizations are derived from both $La_{0.5}Ca_{0.5}MnO_3$ and BFO. Magnetizations taken with a magnetometer show the same manipulation effects in the H2 heterostructure.

This reversible electric control of the magnetic property of a colossal-magnetoresistance manganite was also observed in $PbZr_{0.2}Ti_{0.8}O_3$ (250 nm)/$La_{0.8}Sr_{0.2}MnO_3$ (4.0 nm) heterostructure [55,56]. The magnetic response of the $La_{0.8}Sr_{0.2}MnO_3$ layer together with $PbZr_{0.2}Ti_{0.8}O_3$ can be switched by electric fields, as shown in Fig. 11. It is believed that the large ME coupling effect found in these artificial heterostructures results from an interfacial magnetic reconstruction driven by the charge reversal in $PbZr_{0.2}Ti_{0.8}O_3$ as illustrated in Fig. 11(b).

From the results mentioned above, one can see that clarifying the characteristics of atomic resolution microstructure become increasingly important because the interface situation is crucial for the ME coupling effect. The precise atomically resolved investigations of the interface in artificial heterostructure have risen up [57–60]. By using aberration-corrected scanning transmission electron microscopy (STEM), Taherifind et al. investigated the electric field effect on Mn ionic valance, especially near the interface of the $La_{0.7}Sr_{0.3}MnO_3$/$PbZr_{0.2}Ti_{0.8}O_3$ heterostructure [57]. In the ultrathin limit (<4 nm), strain fluctuations in $La_{0.7}Sr_{0.3}MnO_3$ are minimal and charge-transfer screening drives the ME coupling. The electron energy loss spectroscopy (EELS) maps at the $La_{0.7}Sr_{0.3}MnO_3$/$PbZr_{0.2}Ti_{0.8}O_3$ interface in Fig. 12 reveal the presence of a ~2 nm charge-transfer screening region that gives rise to a change in the local 3*d* band occupancy of Mn, resulting in a deviation from the nominal Mn^{3+}/Mn^{4+} ratio of ~3.3 [61,62]. Both samples with opposite polarization states possess a bulk valence of ~3.4 (near the nominal 3.3), but at the interface the value for the poled-up sample drops to ~2.63, while that for the poled-down sample increases to ~4.26. The valence change is spread over 3–4 unit cells at the interface, with an average valence at ~3.02 for poled-down and ~3.89 for poled-up. However, the magnitude of the induced magnetization is inconsistent with the previous work shown in Fig. 11 [56], suggesting that other factors may be at work. Thus the electric field manipulation on the magnetism of the magnetic films in the multiferroic heterostructures is very complex, and needs further deep investigations.

2.3. Electric field manipulation on the electronic transport properties

In a multiferroic heterostructure, an electric field controls not only the magnetism of magnetic films but also the variations of electronic transport properties. Employing a remanent strain without ferroelectric polarization switching, M. Liu et al. demonstrated that an electric-field-induced two-step ferroelastic switching pathway in (011) oriented PMN-PT substrates could be used to tune the in-plane resistances in epitaxial Fe_3O_4 films [63]. A non-volatile resistance switching in Fe_3O_4 was achieved, driven by two distinct, stable and reversible ferroelastic strain states as shown in Fig. 13. Fig. 13(a) shows *in situ* control of resistances using applied voltages in Fe_3O_4/PMN-PT (011) at different temperatures. Hysteretic changes in resistance were observed upon applying appropriate unipolar electric fields across the PMN-PT substrate, showing a large tunability up to 50% change in resistance. This resistance changes manipulated by electric fields could also be achieved at room temperature, as shown in Fig. 13(b). With appropriate application of unipolar and bipolar electric fields, both the resistance hysteresis loop (blue) and the butterfly-like curve (red) were observed. These results provide a framework for realizing non-volatile switching behaviors of electronic transport coupled to lattice-strain in epitaxial oxide heterostructures over a broad temperature range, with potential device applications.

Besides the strain effect, the interfacial charges have an important impact on the transport properties of magnetic films in multiferroic heterostructures. H. N. Lee et al. fabricated

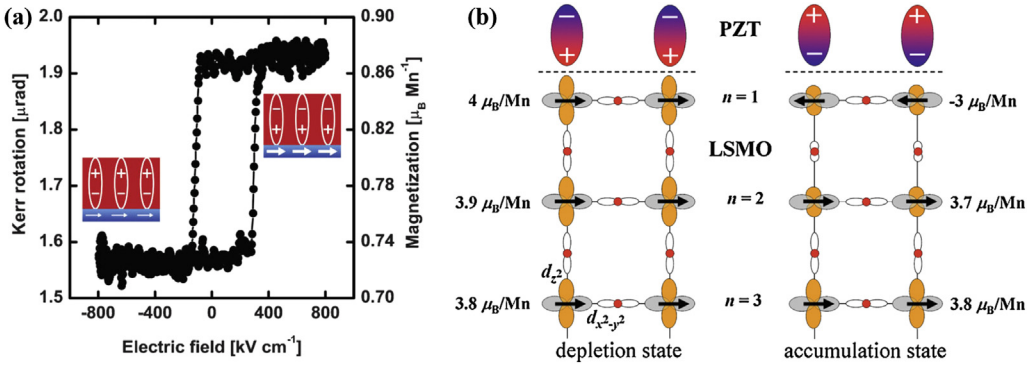

Fig. 11. (a) Magnetoelectric hysteresis curve at 100 K. Insets represent the magnetic and electric states of the $La_{0.8}Sr_{0.2}MnO_3$ and $PbZr_{0.2}Ti_{0.8}O_3$ layers, respectively. Reprinted from Ref. [55]. (b) Schematic model of the spin configurations in $La_{0.8}Sr_{0.2}MnO_3$ at the $PbZr_{0.2}Ti_{0.8}O_3$ interface for the depletion and accumulation states, showing the changes in the Mn and O orbital states and the expected changes in the magnetic moment per layer. The arrows indicate the spin orientations in the Mn cations and n denotes the unit cell number below the $PbZr_{0.2}Ti_{0.8}O_3$. Reprinted from Ref. [56].

different heterostructures composed of the correlated electron oxide $La_{0.8}Sr_{0.2}MnO_3$ with various capping layers on STO substrate as shown in Fig. 14(a), and investigated the electronic transport properties manipulated by interfacial charge effect [64]. The hole accumulation in the ultrathin $La_{0.8}Sr_{0.2}MnO_3$ layer coming from the heterostructure with the ferroelectric layer results in an obvious insulator-metal transition and lower resistivity as shown in Fig. 14(b). The thickness dependent transport properties of $La_{0.8}Sr_{0.2}MnO_3$ films in Fig. 14(c) show that the significant transport difference between the $La_{0.8}Sr_{0.2}MnO_3$ and $PbZr_{0.2}Ti_{0.8}O_3$/$La_{0.8}Sr_{0.2}MnO_3$ heterostructure is strongly related to the manipulation of charge carriers confined to the vicinity of the interface by ferroelectric field effect. Vaz et al. further probed the electronic valence state of Mn in the heterostructure by near edge X-ray absorption spectroscopy as a function of the ferroelectric polarization [56]. It is demonstrated that the large ME response in electronic transport characterization originates

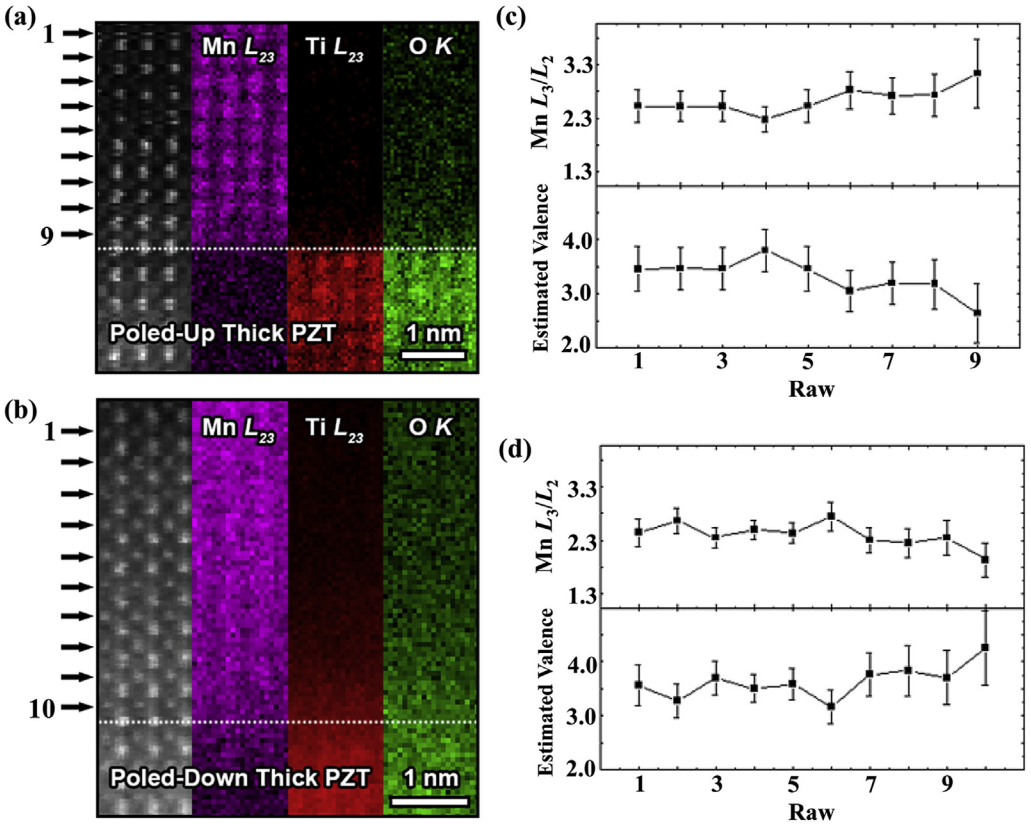

Fig. 12. High-angle annular dark field images and EELS maps of the $La_{0.7}Sr_{0.3}MnO_3$/$PbZr_{0.2}Ti_{0.8}O_3$ interface in (a) poled-up and (b) poled-down thick $PbZr_{0.2}Ti_{0.8}O_3$ sample. (c, d) Calculated Mn L_3/L_2 ratios and estimated Mn valences from each row. Error bars correspond to the standard error of the Gaussian fits to the edges. Reprinted by permission from Ref. [57].

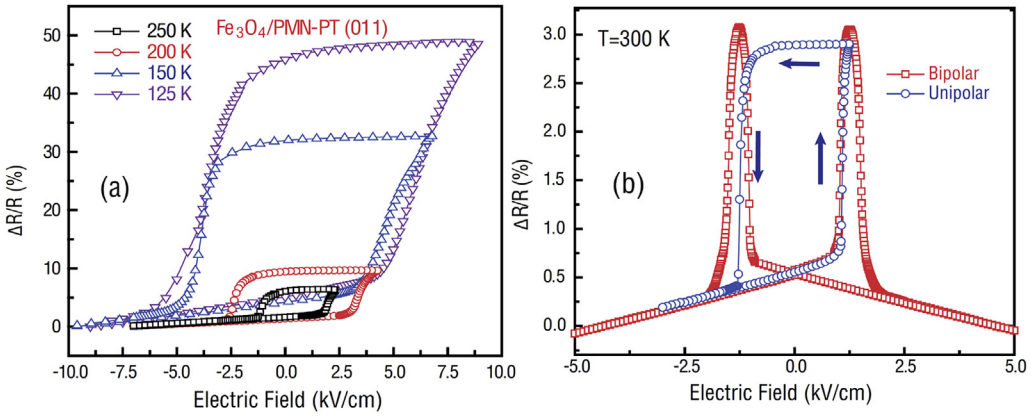

Fig. 13. Non-volatile ferroelastic switching of resistivity in Fe_3O_4/PMN-PT (011). (a) Resistance hysteresis loops at different temperatures. (b) Resistance response under unipolar and bipolar sweeping of electric fields at room temperature. Reprinted by permission from Ref. [63].

from a modified interfacial spin configuration by ferroelectric polarization reversal.

In fact, although the converse piezoelectric and field effects are generally of coexistence, they can be sometimes distinguished. X. G. Li's group realized a programmable electric-field polarizing sequence to separate the volatile and nonvolatile electroresistances related to the converse piezoelectric induced strain and ferroelectric field effects, respectively, in $La_{0.7}Ca_{0.3}MnO_3/SrTiO_3/0.68Pb(Mg_{1/3}Nb_{2/3})O_3$-$0.32PbTiO_3$ heterostructures. The relative contributions of the two effects on the in-plane resistance changes can be quantitatively distinguished by "ON" and "OFF" modes, respectively. For "ON" mode, the resistance of the $La_{0.7}Ca_{0.3}MnO_3$ film is measured with the polarization voltage applied on the substrate. The $R-E$ hysteresis loops in Fig. 15(a–c) have asymmetrical butterfly like shapes at all fixed temperatures, similar to the in-plane piezoelectric curves, suggesting that the manipulation of resistance is strain related. Besides the strain effect, the nonvolatile ferroelectric field effect exists in this mode because of the intrinsic ferroelectric nature of PMN-PT substrate which is confirmed by the asymmetry of the $R-E$ loops. For "OFF" mode, the resistance measurement of the

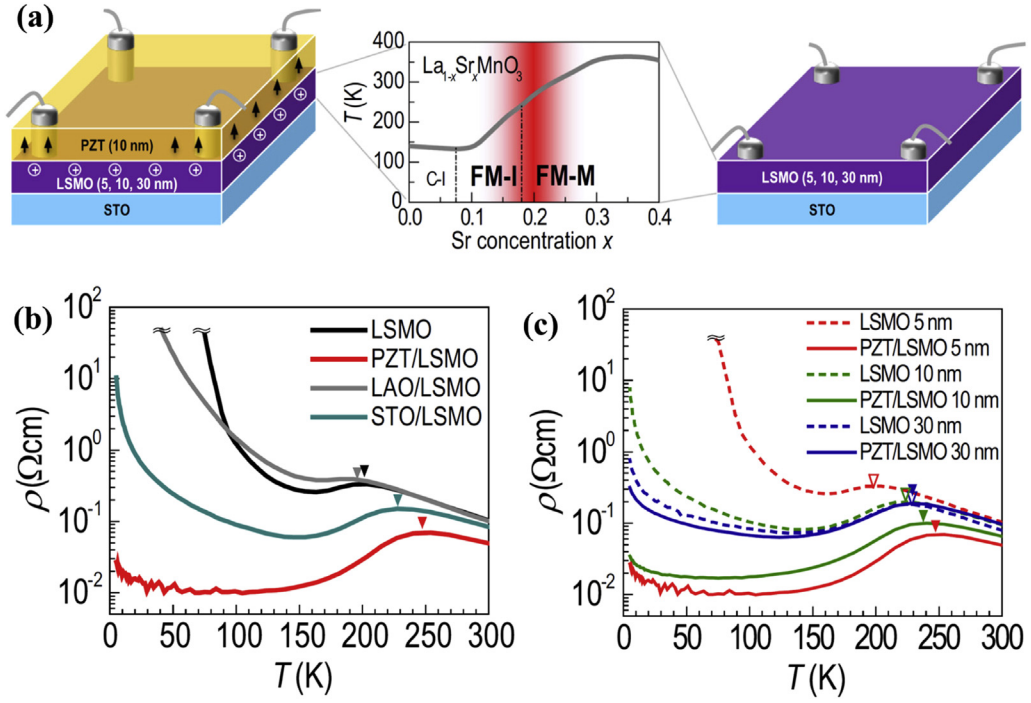

Fig. 14. (a) Left and right schematics represent $PbZr_{0.2}Ti_{0.8}O_3/La_{0.8}Sr_{0.2}MnO_3$ heterostructure and $La_{0.8}Sr_{0.2}MnO_3$ thin film on STO, respectively. The electrodes for in-plane van der Pauw transport measurements were contacted to the $La_{0.8}Sr_{0.2}MnO_3$ layer. The image in the middle shows a part of the phase diagram of $La_{1-x}Sr_xMnO_3$. (b) Temperature-dependent resistivities for ultrathin (5 nm) $La_{0.8}Sr_{0.2}MnO_3$ with 10 nm different capping layers. (c) Temperature-dependent resistivities for different thickness of $La_{0.8}Sr_{0.2}MnO_3$ with or without 10 nm-thick $PbZr_{0.2}Ti_{0.8}O_3$ capping layers. T_C for $La_{0.8}Sr_{0.2}MnO_3$ films are marked with triangles. Reprinted from Ref. [64].

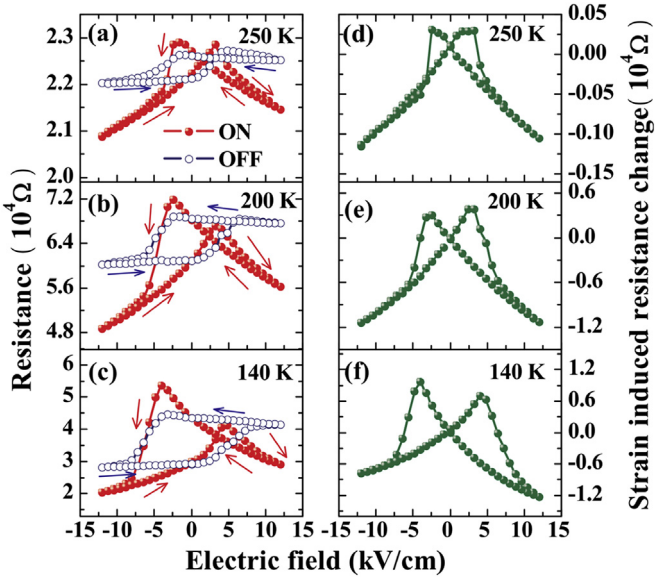

Fig. 15. (a)–(c) Resistances of the $La_{0.7}Ca_{0.3}MnO_3$ films in "ON" and "OFF" modes, respectively, as a function of polarization electric fields applied to PMN-PT single crystal substrate in different temperatures, the arrows indicate the directions of the sweeping fields. (d)–(f) Cycled polarization electric fields dependencies of pure strain induced resistance changes of $La_{0.7}Ca_{0.3}MnO_3$ obtained by subtracting data in "OFF" mode from that in "ON" mode. Reprinted by permission from Ref. [65].

$La_{0.7}Ca_{0.3}MnO_3$ film begins 2 s after the polarization voltage pulse (duration 1 s) is turned off. As the R–E loops in "OFF" mode are induced by field effect while in "ON" mode the loops are induced by both field and strain effects, therefore, the strain effect related resistance change can be obtained by subtracting the resistance values in "OFF" mode from the values corresponding to the same electric field in "ON" mode at the same sweeping direction. As shown in Fig. 15(d–f), the observed symmetrical R–E curves are contributed purely by the strain effect.

3. Multiferroic tunnel junctions

It is known that the electric fields can manipulate not only in-plane resistivities in multiferroic heterostructures but also out-of-plane transport properties, such as resistive switching in switchable ferroelectric diodes or electron tunneling in multiferroic tunnel junctions. Resistive switching in epitaxial ferroelectric heterostructures, which is arisen from the manipulation of band alignment and contact resistance at the ferroelectric/electrode interfaces by switchable ferroelectric polarization, have captured immense interest due to their potential applications such as in nondestructive readout nanoelectronic devices [66–70]. In these ferroelectric diodes, a ferroelectric thin film with the thickness more than 10 nm is sandwiched between two electrodes and the remnant polarization is switched by applying an electric field between the electrodes. As the ferroelectric layer thickness decreases to a few nanometers, electronic conduction is greatly enhanced as quantum-mechanical tunneling through the ferroelectric layer becomes possible [15,71]. These devices in which two electrodes sandwich a ferroelectric tunnel barrier are called ferroelectric tunnel junctions (FTJs).

The basic concept of an FTJ was proposed by L. Esaki et al. decades ago [72], and it aroused a considerable research interest recently due to the fact that ferroelectricity can persist down to the nanometer scale [73–75]. One of the key points for an FTJ is the junction resistance switching based on the ferroelectric polarization reversal, leading to the tunneling electroresistance (*TER*) effect that can be expressed as follows

$$TER = (R_{high} - R_{low})/R_{low} \quad (1)$$

where R_{high} and R_{low} are defined as the high and low resistances corresponding to the opposite ferroelectric polarization directions, respectively, for an FTJ schematically shown in Fig. 16(a). Taking the advantages of scanning probe technique [76], large *TER* effects have recently been demonstrated on bare surfaces of ultrathin ferroelectrics such as BTO [77–80] and $PbZr_xTi_{1-x}O_3$ [81–83] ferroelectric films using a conductive atomic force microscope tip as top electrode. More importantly, the giant *TER* ratios at room temperature have been demonstrated in the FTJs with a capacitor-like geometry [84–86], which is very important for practical applications in memory cells.

For quantum-mechanical tunneling nanojunctions, magnetic tunnel junctions (MTJ), which consists of two ferromagnetic metal layers separated by a thin insulating barrier, see Fig. 16(b), have aroused considerable interest and been most widely used in spintronic devices such as computer read heads, sensors, and memories [87–90]. The parallel (P) and antiparallel (AP) magnetization alignments of the two magnetic electrodes in an MTJ, representing two logic states with different resistances, has the tunneling magnetoresistance (*TMR*) effect as

$$TMR = (R_{AP} - R_P)/R_P \quad (2)$$

where R_P and R_{AP} denote the resistances in the parallel and antiparallel magnetic configurations, respectively [91]. Recently, the electric field driven magnetization switching has been realized in an MTJ without an applied magnetic field utilizing ME coupling at the interface, which may provide a pathway of electric filed manipulated transport across heterostructures [92].

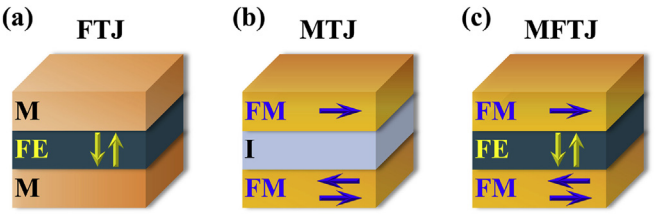

Fig. 16. Schematic view of the different types of tunnel junctions: (a) FTJ, (b) MTJ, and (c) MFTJ. Ferroelectric (FE), metal (M), ferromagnetic (FM), and insulating (I) layers are indicated where appropriate.

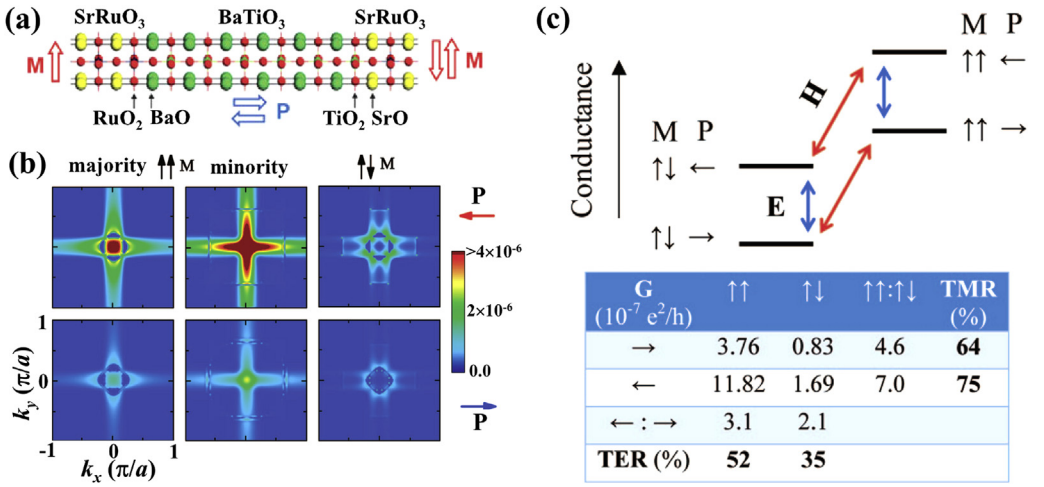

G (10^{-7} e^2/h)	↑↑	↑↓	↑↑:↑↓	TMR (%)
→	3.76	0.83	4.6	**64**
←	11.82	1.69	7.0	**75**
←:→	3.1	2.1		
TER (%)	**52**	**35**		

Fig. 17. (a) Schematic illustration of atomic structure of the SRO/BTO/SRO MFTJ with asymmetric interfaces. (b) Transmission in the two-dimensional Brillouin zone of the MFTJ. (c) Conductance of the SRO/BTO/SRO MFTJ. The four conductance states are distinguished by polarization in the barrier pointing to the left (←) or right (→) and magnetizations of the electrodes being parallel (↑↑) or antiparallel (↑↓). The diagram on the top schematically shows the four resistance states and the table on the bottom gives the related *TMR* and *TER* ratios. Reprinted by permission from Ref. [97].

Based on the progresses mentioned above, multiferroic tunnel junctions, namely, MFTJs, which refer to MTJs with ferroelectric barriers or the FTJs with ferromagnetic electrodes, are proposed [93,94], as illustrated in Fig. 16(c). Such a ferromagnetic/ferroelectric/ferromagnetic (FM/FE/FM) MFTJ is expected to be characterized by the *TMR* and *TER* simultaneously, and such an MFTJ thus exhibits four resistance states in a single memory unit cell, which inevitably receives much attentions as the next generation of information storages [15,95,96].

3.1. Four resistance states in MFTJs

In 2009, J. P. Velev et al. theoretically predicted that an FM/FE/FM MFTJ, such as $SrRuO_3/BaTiO_3/SrRuO_3$ (SRO/BTO/SRO) heterostructure, should be of four resistance states [97]. Fig. 17(a) illustrates the atomic structure of the predicted MFTJ with a tunneling barrier BTO film having different interface terminations, *i.e.*, BaO at the left and TiO_2 at the right interface. Thus, the different interface terminations have different energies for two polarization states, making the potential profile asymmetric. In other words, the asymmetric interfaces will provide a necessary requirement for observing the *TER* effect even with two same electrodes. While for the *TMR* in SRO/BTO/SRO MFTJ, it depends on the magnetic configurations of two ferromagnetic SRO electrodes. In a parallel magnetic configuration, the majority-spin and minority-spin channels contribute to the conductance, whereas in antiparallel magnetic configuration the conductance is strongly suppressed due to symmetry mismatch, resulting a *TMR* effect. The transmission in the two-dimensional Brillouin zone of the SRO/BTO/SRO MFTJ is shown in Fig. 17(b). It is obvious that the transmission strongly depends on polarization states and magnetic configurations. Correspondingly, the schematic illustration and calculated values of four conductance levels are given in Fig. 17(c). The calculated *TMR* and *TER* ratios depend on the polarization and magnetization states, respectively, indicating the signature of a true multifunctional device.

3.2. ME coupling in MFTJs

3.2.1. MFTJs with oxide/metal interface

Soon after the theoretical predictions, such FM/FE/FM MFTJs with four-state resistances were experimentally investigated. By means of a Fe indentation technique, V. Garcia et al. had fabricated the nanoscale Fe (or Co)/$BaTiO_3$/$La_{0.7}Sr_{0.3}MnO_3$ FM/FE/FM MFTJs on the $NdGaO_3$ substrate with the tunneling barrier BTO having thickness of 1 nm and demonstrated the control of spin polarization by electrically reversing the ferroelectric polarization [98]. The typical resistance *vs.* magnetic field curves measured at 4.2 K and −50 mV bias voltage show that the MFTJ with the ferroelectric barrier BTO poled up has a negative *TMR* about −17%, as shown in Fig. 18. More interestingly, when switching the ferroelectric polarization of a tunnel barrier with voltage pulses, the *TMR* value was depressed to a low one about −3%. Because the spin polarization of half-metallic $La_{0.7}Sr_{0.3}MnO_3$ is insensitive to the ferroelectric polarization direction, a large interfacial modifications of the spin polarization are expected through *ab* initio calculations of 3*d* electronic states of Fe at the Fe/BTO interface [99,100]. Thus, the change in *TMR* is closely related to the variations of spin polarization of the Fe/BTO interface induced by the ferroelectric polarization. To quantificationally evaluate the interfacial ME coupling effect in MFTJs, the tunnel electromagnetoresistance (*TEMR*) is proposed as

$$TEMR = (TMR_{\text{high}} - TMR_{\text{low}})/TMR_{low} \quad (3)$$

where TMR_{high} and TMR_{low} denote the high and low *TMR* ratios corresponding to the opposite ferroelectric polarization directions, respectively. Accordingly, the obtained *TEMR*

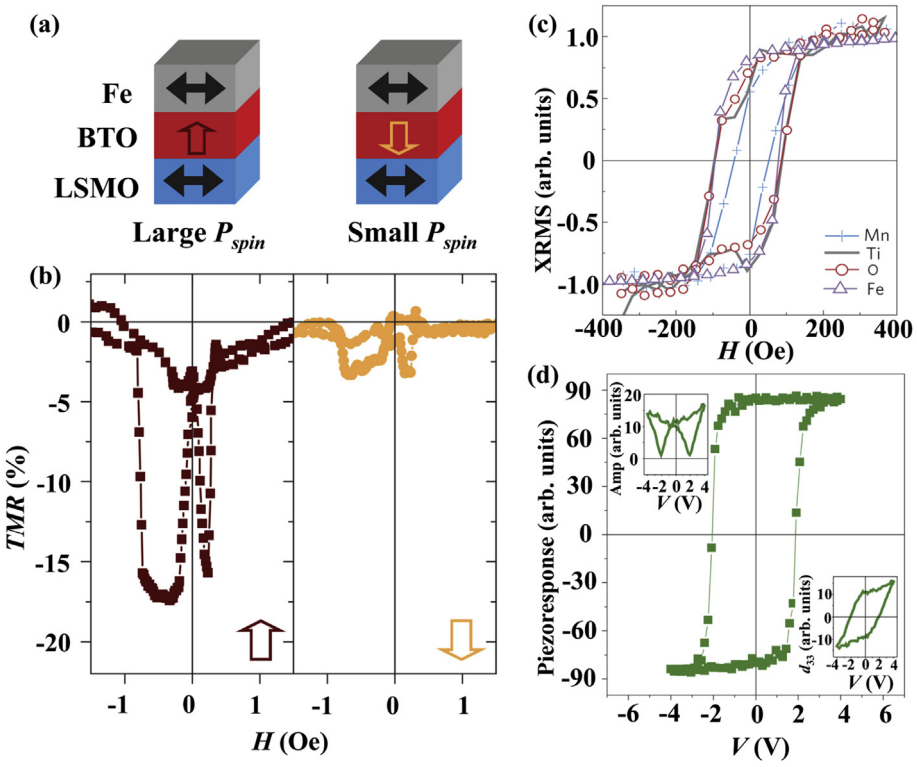

Fig. 18. (a) Device schematic with horizontal and longitudinal arrows to indicate magnetizations and ferroelectric polarization directions, respectively. (b) R–H curves for Fe/$BaTiO_3$/$La_{0.7}Sr_{0.3}MnO_3$ MFTJ after poling the ferroelectric up or down at $T = 4.2$ K. (c) XRMS *vs*. H for Mn, Fe, Ti and O for the Fe/BTO sample. Reprinted by permission from Ref. [98]. (d) Out-of-plane piezoresponse phase loop of a $BaTiO_3$ (1.2 nm)/$La_{0.7}Sr_{0.3}MnO_3$ sample, and the insets show the corresponding amplitude and extracted piezoelectric coefficient (d_{33}). Reprinted by permission from Ref. [101].

~450% suggests the presence of a strong interfacial ME coupling in the MFTJ.

This interfacial ME coupling effect at Fe/BTO interface in Fe/$BaTiO_3$/$La_{0.7}Sr_{0.3}MnO_3$ can be confirmed by using soft X-ray resonant magnetic scattering (XRMS) and piezoresponse force microscopy (PFM) [101]. It is revealed that, at the interface with Fe, ultrathin films of the archetypal ferroelectric BTO simultaneously possess the magnetizations and the polarizations at room temperature in the MFTJs. Fig. 18(c) shows the magnetic field dependencies of XRMS signals at selected energies. All signals show clear hysteresis loops as the functions of magnetic fields. It is noteworthy that Ti and O signals reverse at the same magnetic field as Fe, indicating that the magnetic moments carried by the Ti and O ions are coupled to the Fe at the interface. Fig. 18(d) shows the out-of-plane piezoresponse of a similar $BaTiO_3$ (1.2 nm)/$La_{0.7}Sr_{0.3}MnO_3$ sample as a function of the applied voltages, confirming a ferroelectric character in the ultrathin BTO film.

By means of atomically resolved real-space spectroscopic techniques STEM and EELS, L. Bocher et al. further probed the nanoscale structural and electronic modifications at the Fe/BTO interface in Fe/$BaTiO_3$/$La_{0.7}Sr_{0.3}MnO_3$ MFTJs, as shown in Fig. 19 [102]. It was found that there is an additional FeO monolayer intercalated between BTO and Fe, which is different from the previously theoretical prediction [99]. Based on this accurate observation of the interface, an atomistic model for the Fe/BTO interface was proposed, as shown in Fig. 19(a). This ultrathin oxidized iron layer sandwiched between BTO and Fe was also reported by G. Radaelli et al. through XMCD [103]. It was demonstrated that the magnetization of the oxidized iron layer at the Fe/BTO interface can be electrically and reversibly switched "on" and "off" at room temperature by reversing polarization of BTO. As shown in Fig. 19(b), the dichroic signal of FeO_x has been suppressed for poling ferroelectric polarization downward (P_{dn}) compared to that for poling upward (P_{up}). The results indicate that for P_{dn} the FeO_x interface will undergo a magnetic transition towards an AFM (or paramagnetic) state, while for P_{up} the FeO_x interface remains robustly FM state.

Due to the ME coupling at such a multiferroic interface, the magnitudes and the signs of the *TMR* could be changed by ferroelectric switching as reported in Co/$PbZr_{0.2}Ti_{0.8}O_3$/$La_{0.7}Sr_{0.3}MnO_3$ MFTJs by D. Pantel et al. [104]. Fig. 20(a) shows the resistance *vs*. magnetic field curves for the MFTJ with an appropriate $PbZr_{0.2}Ti_{0.8}O_3$ thickness of 3.2 nm measured at $V_{DC} = 10$ mV and 50 K. When switching the polarization from pointing towards Co (polarization poled up) to pointing towards $La_{0.7}Sr_{0.3}MnO_3$ (polarization poled down) by applying a voltage pulse, besides the resistance of the junction is modified, the *TMR* is switched from inverse (−3%) to normal (+4%). Although the values of *TMR* are low possibly because of the defects within the barrier or different interface structures at the Co/PZT interface with the large junction area (4000 μm^2), the corresponding *TEMR* reaches

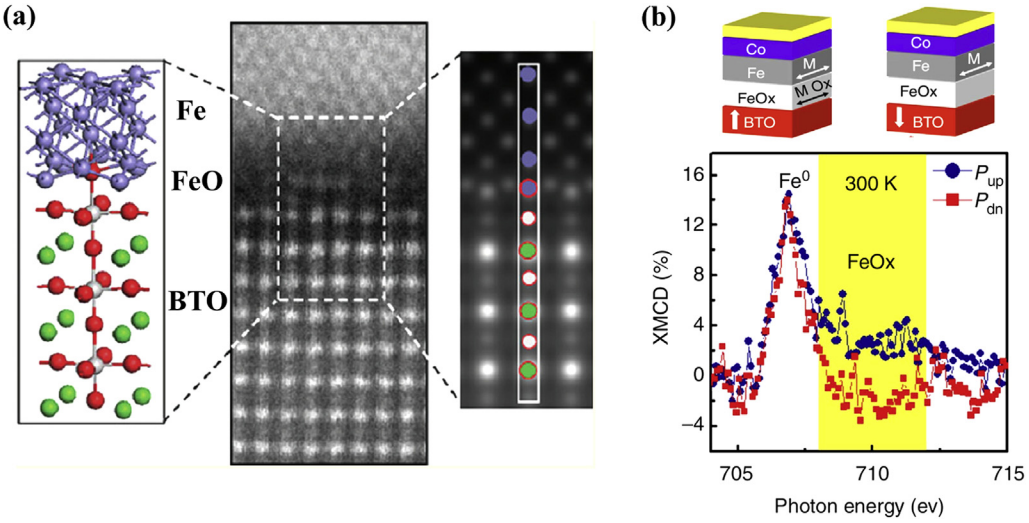

Fig. 19. (a) The high-angle annular dark-field images and the interface model of Fe/BTO heterostructure. Reprinted by permission from Ref. [102]. (b) The schemes of the Fe/BTO interfaces for P_{up} and P_{dn}, and the XMCD signals in the Fe–L_3 energy region for BTO polarization P_{up} (blue circles) and P_{dn} (red squares) for capacitors at 300 K. Reprinted from Ref. [103].

about −230%, providing potential for electrically controlled spintronic devices. Furthermore, the signs of the *TMR* could be reversibly inverted by switching ferroelectric polarization of the barrier, as summarized in Fig. 20(b). This effect is most probably related to the strong ME coupling at Co/$PbZr_{0.2}Ti_{0.8}O_3$ interface, which could be ascribed to the hybridization at the interface, or spin-dependent screening in the magnetic electrode, but not observed at the $PbZr_{0.2}Ti_{0.8}O_3$/$La_{0.7}Sr_{0.3}MnO_3$ interface.

Another way to obtain multi resistance states in a single device unit cell is to employ a single phase multiferroic material as the tunnel barrier. Taking the advantages of the coexistence of electric and magnetic orders in the singular multiferroics $La_{0.1}Bi_{0.9}MnO_3$, M. Gajek et al. [105] had experimentally demonstrated a kind of MFTJ, Au/$La_{0.1}Bi_{0.9}MnO_3$ (2 nm)/$La_{0.7}Sr_{0.3}MnO_3$. In this MFTJ, the *TMR* arises from the spin filtering effect and the *TER* originates from the reversing of the ferroelectric polarization of $La_{0.1}Bi_{0.9}MnO_3$. Owing to the coexistence of *TMR* and *TER* effects, the MFTJ shows a four-state resistance which could be switched by both electric and magnetic fields. When the ferroelectric polarization of $La_{0.1}Bi_{0.9}MnO_3$ point towards $La_{0.7}Sr_{0.3}MnO_3$, two resistance states of "1" and "2" were obtained in such a MFTJ when the magnetization of $La_{0.1}Bi_{0.9}MnO_3$ was set parallel and antiparallel to that of $La_{0.7}Sr_{0.3}MnO_3$, respectively, as shown in Fig. 21. After reversing the ferroelectric polarization of $La_{0.1}Bi_{0.9}MnO_3$, the entire *R*–*H* curve shifts so that both P and AP resistances switched to different values to form the other two resistance states of "3" and "4".

3.2.2. All-perovskite-type MFTJs

From the results mentioned above, we note that metals (Fe and Co) tend to be oxidized to form a dielectric layer at the electrode/barrier interface, which, to some extent, can provide a significant contribution to the behaviors of resistance versus ferroelectric polarization in MFTJs [102,103]. In addition, such a metallic oxide dielectric layer may present an antiferromagnetic state [103], which suppresses spin-dependent tunneling and thus *TMR* effect. On the other hand, the

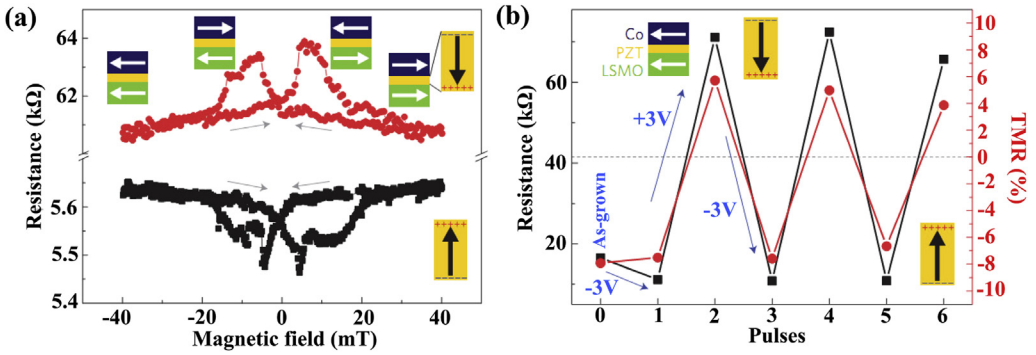

Fig. 20. (a) Resistance *vs*. magnetic field curves for a Co/$PbZr_{0.2}Ti_{0.8}O_3$ (3.2 nm)/$La_{0.7}Sr_{0.3}MnO_3$ junction measured at 50 K with the ferroelectric polarization pointing upward (black curve) and downward (red curve). (b) Resistance (black squares) and *TMR* (red circles) after successive switching with ±3 V voltage pulses at 10 K. Reprinted by permission from Ref. [104].

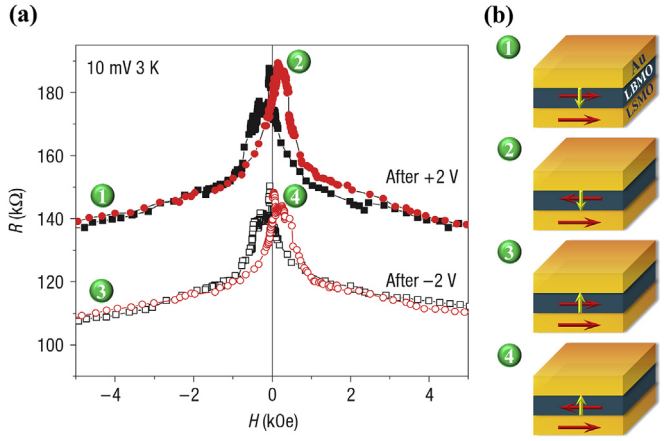

Fig. 21. (a) Tunnel magnetoresistance curves at 3 K at V_{DC} = 10 mV in the Au/$La_{0.1}Bi_{0.9}MnO_3$ (2 nm)/$La_{0.7}Sr_{0.3}MnO_3$ MFTJ after applying voltages of +2 V (filled symbols) and −2 V (open symbols). (b) Schematic of different magnetization and polarization states for the corresponding four resistance states. Reprinted by permission from Ref. [105].

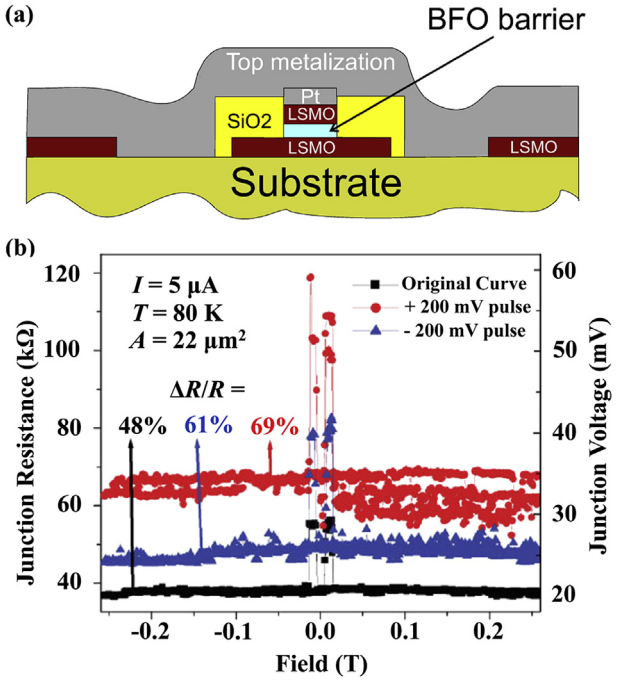

Fig. 22. (a) Side view of the stack showing the BFO barrier sandwiched with $La_{0.67}Sr_{0.33}MnO_3$ electrodes and surrounded by insulating SiO_2. (b) *TMR* from a junction showing the interface-mediated magnetoelectric effect after ±200 mV bias pulses. Reprinted by permission from Ref. [110].

fatigue, aging, and imprint of ferroelectric thin films grown on normal metal bottom electrodes give rise to the consequence that the devices would not have reliable performances for a long time due to the nonideal interfaces between ferroelectric layers and normal metal electrodes [106]. To avoid the deficiency mentioned above, the lanthanum manganites $La_{1-x}A_xMnO_3$ (A = Ca, Sr) have been chosen as electrodes for the epitaxial perovskite heterostructures, owning to their lattice matched with perovskite ferroelectrics and metallic conductivity [67,107–109]. Therefore, a MFTJ composed of full-perovskite-type oxides offers an ideal platform for investigating the interplay between electrical polarization and tunneling magnetoresistance.

The all-perovskite-type MFTJ with four resistance states related to the magnetization alignment of the electrodes (*TMR*) and the polarization orientation in the ferroelectric barrier (*TER*) was first experimentally observed by M. Hambe et al. [110]. They chose BFO as the ferroelectric barrier and half-metallic manganite $La_{0.67}Sr_{0.33}MnO_3$ as the top and bottom ferromagnetic electrodes to form entirely all-oxide $La_{0.67}Sr_{0.33}MnO_3$/$BiFeO_3$ (~3 nm)/$La_{0.67}Sr_{0.33}MnO_3$ MFTJ, as shown in Fig. 22(a). In an initial state, the observed *TMR* ratio is about 48% in a 22 μm^2 MFTJ measured at a constant bias current of 5 μA and T = 80 K. The voltage pulses of ±200 mV applied across the junction lead to considerable variations of the *TMR* ratios as well as the resistances at parallel electrode magnetizations indicating a interface-mediated magnetoelectric effect [97], as shown in Fig. 22(b). The *TMR* ratios of the junction are 69% and 61% at pulses with +200 mV and −200 mV, respectively, and the corresponding *TEMR* ratio is about 13%.

It should be pointed that due to the interfacial exchange coupling effect, the antiferromagnetic order in BFO makes it possible to have exchange bias effect in ferromagnetic/BFO heterostructures [111,112]. However, in MFTJ trilayer heterostructure fabricated by M. Hambe et al. [110], no exchange bias effect had been found probably because of very thin BFO (2.6 nm) film. In order to confirm the exchange bias phenomenon in BFO-based junction, X. G. Li's group had fabricated high quality epitaxial $La_{0.6}Sr_{0.4}MnO_3$ (25 nm)/$BiFeO_3$ (10 nm)/$La_{0.6}Sr_{0.4}MnO_3$ (50 nm) MFTJs on (001) $(LaAlO_3)_{0.3}(SrAl_{0.5}Ta_{0.5}O_3)_{0.7}$ substrates by a magnetron sputtering technique [113]. It is clear that, besides four resistance states, the exchange bias effect was found in the junctions. Fig. 23(a) shows the *M-H* loops of the as-grown trilayer $La_{0.6}Sr_{0.4}MnO_3$/$BiFeO_3$/$La_{0.6}Sr_{0.4}MnO_3$ with a magnetic field of 5000 Oe cooling from 400 K to different selected temperatures. A negative exchange bias field H_{EB} about −60 Oe at 10 K was observed. Fig. 23(b) shows the exchange bias fields H_{EB} are about −74 Oe for negative polarized state and −72 Oe for positive polarized state, respectively, in the MFTJ with the size of 10 × 10 μm^2. The *TMR* values are 6.6% and 5.6% for the negative and positive polarization states, respectively, and the corresponding *TEMR* ratio is 18% which is larger than that of the similar MFTJ with BFO as the ferroelectric barrier in earlier report [110]. However, the values of *TEMR* in the BFO-based junctions are much smaller than that of Fe/$BaTiO_3$/$La_{0.7}Sr_{0.3}MnO_3$ [98] and Co/$PbZr_{0.2}Ti_{0.8}O_3$/$La_{0.7}Sr_{0.3}MnO_3$ [104], which may be ascribed to the antiferromagnetic order and high leakage current of BFO barrier.

In spite of that all of MFTJs mentioned above work only at relatively low temperatures, fortunately, a room-temperature four-nonvolatile state device had been reported in an all-perovskite-type oxides $La_{0.7}Sr_{0.3}MnO_3$/(Ba, Sr)TiO_3/$La_{0.7}Sr_{0.3}MnO_3$ MFTJ (~10 μm × 20 μm in area) [114]. Fig. 24(a) shows the magnetic field dependences of the junction resistances for the MFTJ with two opposite ferroelectric

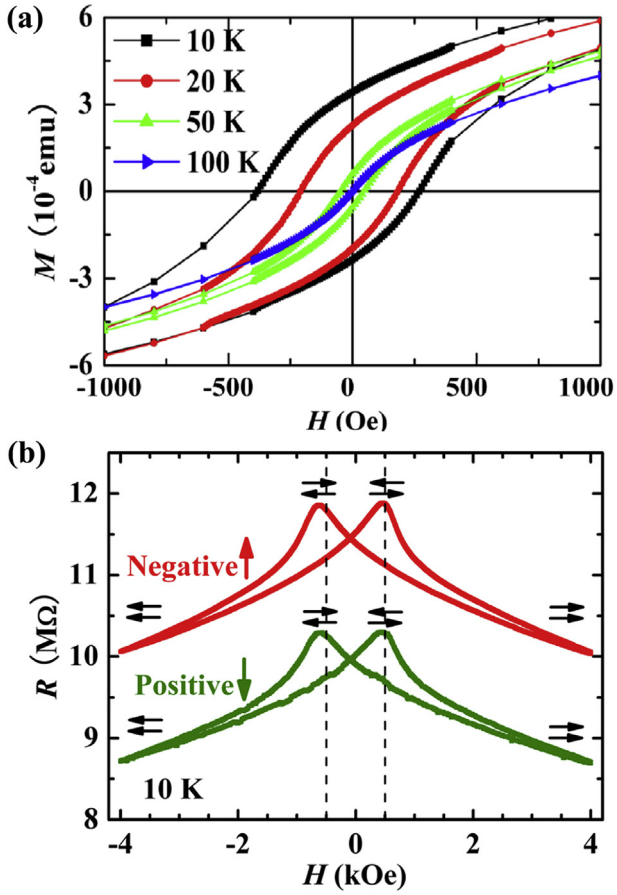

Fig. 23. (a) Magnetic hysteresis loops at different temperatures for the unpatterned $La_{0.6}Sr_{0.4}MnO_3/BiFeO_3/La_{0.6}Sr_{0.4}MnO_3$ trilayers with magnetic field of 5000 Oe cooling from 400 K to selected temperatures. (b) $R-H$ curves of the $La_{0.6}Sr_{0.4}MnO_3/BiFeO_3/La_{0.6}Sr_{0.4}MnO_3$ MFTJ measured at 10 K with positive (olive downward-pointing arrows) and negative (red upward-pointing arrows) polarizations. The black horizontal arrows indicate the directions of magnetizations for the two FM electrodes, and the dashed lines are guide to the eyes. Reprinted by permission from Ref. [113].

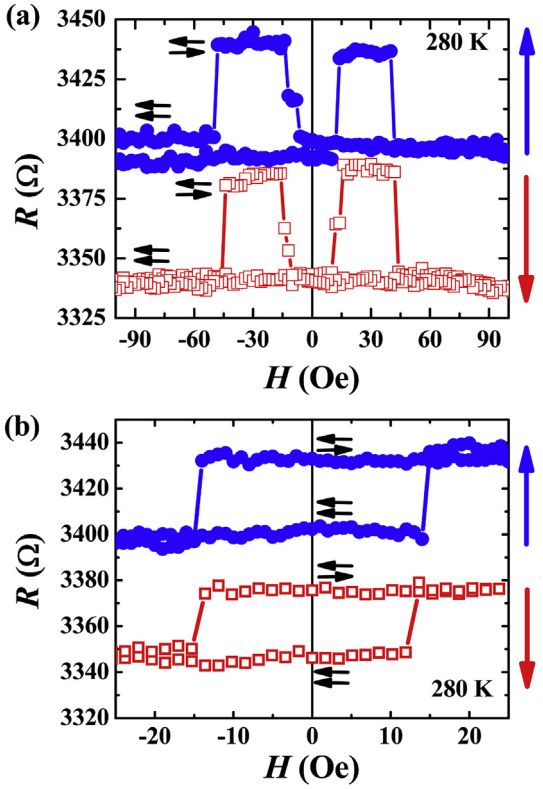

Fig. 24. R *vs.* H between (a) ±100 Oe, and (b) ±30 Oe for a $La_{0.7}Sr_{0.3}MnO_3/(Ba, Sr)TiO_3/La_{0.7}Sr_{0.3}MnO_3$ MFTJ measured at 10 mV and 280 K after poling the ferroelectricity upward (red) and downward (blue). The horizontal arrows indicate the directions of the electrode magnetizations and the vertical arrows indicate the directions of the barrier polarization. Reprinted by permission from Ref. [114].

polarization states measured at 10 mV and 280 K. A sharp resistance change between parallel and antiparallel magnetization alignments suggests an almost entire flip of the magnetic domains. One can see that the entire $R-H$ curve shifts when switching the ferroelectric polarization orientations, namely, the resistances for both parallel and antiparallel magnetization alignments switch to different values and four resistance states appear. Standard MTJ memory loops, as shown in Fig. 24(b), can also be obtained for both polarization states. These four distinct states observed at zero magnetic and electric fields indicate a non-volatile MFTJ memory with four states in a single memory cell is achieved. Fig. 25 shows the resistances (measured at 10 μA bias and 295 K) with different magnetization alignments in response to applied voltage pulses, indicating that the junction resistances can be repeatedly switched by reversing barrier polarization.

3.2.3. Magnetoelectrically enhanced TER in MFTJ

Actually, the small *TER* ratio of 2% in $La_{0.7}Sr_{0.3}MnO_3/(Ba, Sr)TiO_3/La_{0.7}Sr_{0.3}MnO_3$ MFTJ shown in Fig. 24 is too small to be applicable. To enhance the *TER* effect in all-perovskite MFTJs, Yin et al. [115]. had designed and fabricated epitaxial $La_{0.7}Sr_{0.3}MnO_3$ (30 nm)/$La_{0.5}Ca_{0.5}MnO_3$(0.4–1.2 nm)/$BaTiO_3$ (3 nm)/$La_{0.7}Sr_{0.3}MnO_3$ (50 nm) MFTJ with a inserted thin layer $La_{0.5}Ca_{0.5}MnO_3$ between the ferromagnetic $La_{0.7}Sr_{0.3}MnO_3$ top electrode and ferroelectric BTO barrier according to the theoretical prediction proposed by Burton and Tsymbal [116], as schematically shown in Fig. 26(a). For the polarization pointing to the thin $La_{0.5}Ca_{0.5}MnO_3$ layer [see Fig. 26(b)], the screening electron accumulation or hole depletion will change the doping level of $La_{0.5}Ca_{0.5}MnO_3$ to $x < 0.5$ side which is in ferromagnetic metallic phase [117]. While at the other side of BTO barrier, because the stoichiometry of $La_{0.7}Sr_{0.3}MnO_3$ is far away from the phase boundary, the theoretical calculation demonstrated that the magnetic reconstruction will not occur [118]. If the polarization pointing away from $La_{0.5}Ca_{0.5}MnO_3$ film, the electron depletion or hole accumulation will change $La_{0.5}Ca_{0.5}MnO_3$ to $x > 0.5$ side and push it into antiferromagnetic insulating phase. A few unit-cells of antiferromagnetic $La_{0.5}Ca_{0.5}MnO_3$ may act as an atomic-scale spin valve by filtering spin-dependent current and change the junction resistances a great deal. Thus, a much larger *TER* effect could be observed.

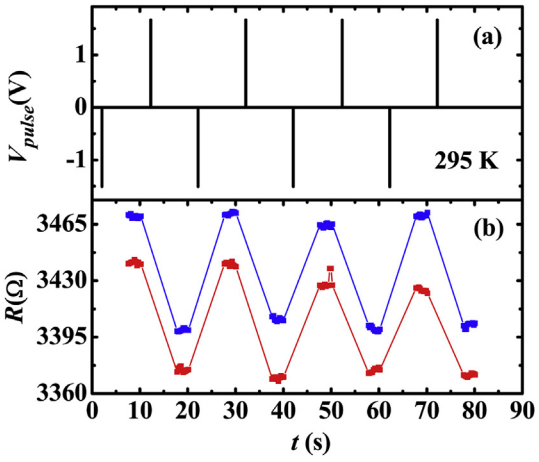

Fig. 25. (a) Applied voltage pulses and (b) repeatable switching of the junction resistances (measured at 10 μA) for a $La_{0.7}Sr_{0.3}MnO_3$/(Ba, Sr)TiO_3/$La_{0.7}Sr_{0.3}MnO_3$ MFTJ at parallel (red) and antiparallel (blue) states. Reprinted by permission from Ref. [114].

Fig. 26(c) shows the resistance memory loop as a function of pulsed poling voltage for an MFTJ with 2 unit cells $La_{0.5}Ca_{0.5}MnO_3$ inserted, labeled as S1. Each datum point in the hysteresis curve was collected at a fixed bias voltage of 10 mV after applying a voltage pulse (V_{pulse}) at 40 K. The *TER* ratio reaches up to ~5000% and is much larger than those in the previous reported MFTJs [98,110,114,119]. For comparison, the *R*-V_{pulse} loop of another junction without $La_{0.5}Ca_{0.5}MnO_3$ inserted, labeled as S2, was also measured, and the *TER* ratio for this junction is only ~30% which is much smaller than S1, as shown in Fig. 26(d). Besides, the *TER* values for the both junctions decrease with increasing temperature and become very small (a few per cent) above 180 K. The drop of *TER* with increasing temperature is related to the following aspects: i) the defect-mediated inelastic tunneling enabled at temperatures above 180 K [120]. ii) the unsaturated ferroelectric state and a decrease in the polarization amplitude.

4. Prospect

4.1. Ferroelectric controlled MTJ

Based on the discussions mentioned above, one can see that the electric writing of the magnetic and electric information in spintronic devices, such as MTJs, would be a promising future memory. J. M. Hu et al. [121] used phase-field simulations to study the piezoelectric and ME responses in a three dimensional multiferroic nanostructure consisting of a perpendicularly magnetized nanomagnet Ni

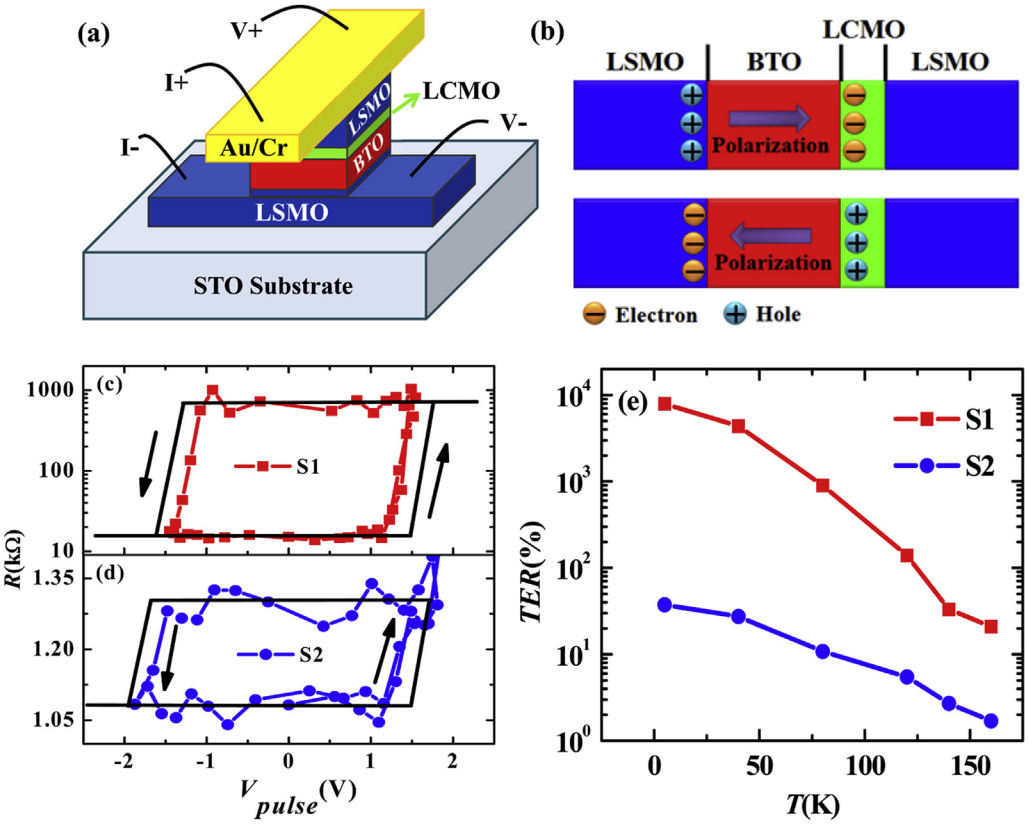

Fig. 26. (a) Schematic diagram of the MFTJ device configuration. (b) Schematic illustration of the screening charge accumulation in electrodes for opposite ferroelectric polarization orientations in the BTO layer. (c–d) The resistance memory loops as the functions of pulsed poling voltages (V_{pulse}) at 40 K for MFTJs with (c) and without (d) $La_{0.5}Ca_{0.5}MnO_3$ inserted. The solid lines are the guide to the eyes. The arrows indicate the direction of pulse sequence. (e) Temperature dependent *TER* for junctions S1 and S2 measured at 10 mV. Reprinted by permission from Ref. [115].

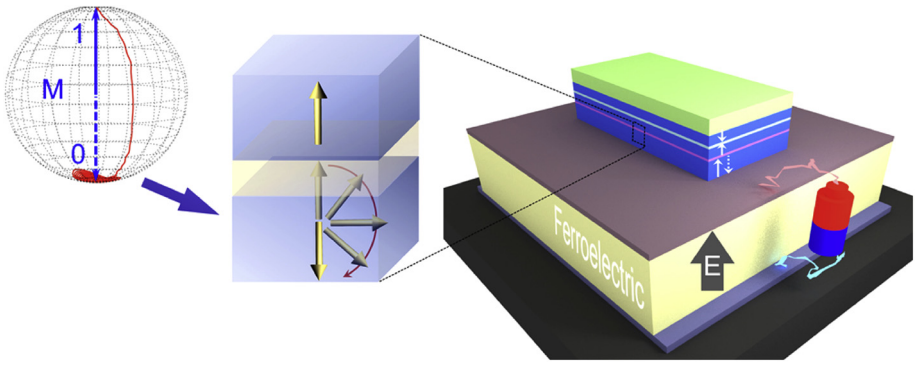

Fig. 27. (Left panel) Spatial trajectories of precessional magnetization switching in polycrystalline Ni upon applying electric-fields across the multiferroic heterostructure. (Middle panel) Schematic illustration of a perpendicularly magnetized MTJ, consisting of a dielectric tunnel barrier sandwiched by a pinned layer with a fixed perpendicular magnetization and a free layer where the perpendicular magnetization reversal occurs. (Right panel) Schematic diagram of a prototype device with MTJ deposited on a ferroelectric substrate. Reprinted by permission from Ref. [121].

with an in-plane long axis and a juxtaposed ferroelectric nanoisland $Pb(Zr,Ti)O_3$, as shown in Fig. 27. A nonvolatile, repeatable and electrically driven perpendicular magnetization reversal is modeled by applying an electric field pulse with a certain duration. The proposed reversal path by successive precession and damping is achieved based on the strain-mediated volatile electrically induced reorientation of the perpendicular easy-axis to the in-plane long axis of a nanomagnet. In contrast to previous reports [37,122–124], the advantages of this three dimensional multiferroic nanostructure are as follows. i) Neither static nor dynamic magnetic fields are required for this reversal. ii) Because only unipolar electric fields are applied across ferroelectrics, there is no full polarization reversal, hence the ferroelectric fatigues can be greatly alleviated [125]. Furthermore, a wide tunable range (from 1.3 ns up to 31 ns, or even longer under smaller damping coefficients) of the electric field pulse duration is exhibited, providing great flexibility for experimental verifications and device designs.

Fig. 28 shows a strain mediated multi-memory state MTJ [41]. It is noted that the magnetization of the strain controlled Co layer (M_S) can be manipulated by a voltage V_{write}, while the magnetization of another Co layer (M_S') pinned by an antiferromagnetic layer is hardly rotated, thus the device forms three resistance states revealed by measuring V_{read}. Via electric field control, the M_S will reversibly change between parallel and perpendicular states with respect to the M_S', where the symbol "⊗" shown in Fig. 28(b) denotes the M_S perpendicular to the M_S'. In addition, via a small auxiliary magnetic field (5 Oe), the antiparallel alignment can also be achieved, which

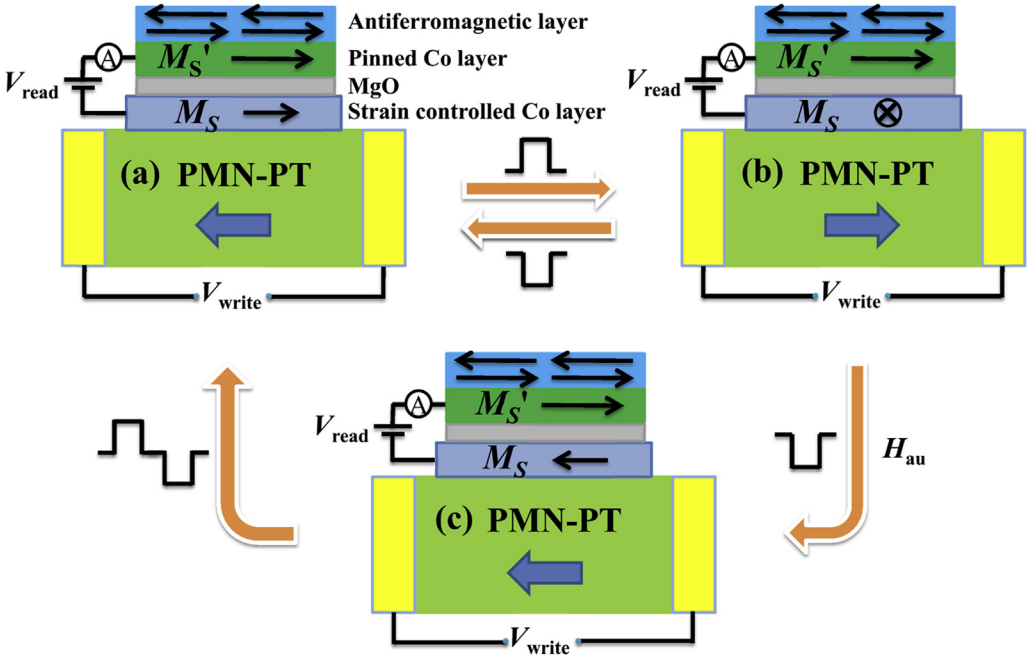

Fig. 28. An MTJ prototype device controlled by electric fields with three resistance states due to three magnetization configurations: (a) parallel state, (b) perpendicular state and (c) antiparallel state. Reprinted by permission from Ref. [41].

results in an electrically controlled tri-state MTJ to enhance the storage density. If MgO barrier layer in Fig. 28 is replaced by a ferroelectric, then the device should have at least six resistance states in this MFTJ.

4.2. Octonary resistance states in MFTJs

The demands for faster, smaller, and non-volatile electronic devices have led to an emergent need to develop new concepts for information processing and storage. Theoretically, combining the spin-filter effect and the screening of polarization charges between two ferromagnetic electrodes through a general spintronic tunneling, eight different logic states can be produced by using single phase multiferroic materials as tunneling barriers in MFTJs [126]. Compared to the binary memory, the octal codes using the eight-resistance-state MFTJ can greatly increase the capacity of data storage. However, most of the single phase multiferroic materials show antiferromagnetism [13]. Thus, to realize the applications of MFTJ with eight-resistance-state, on the one hand it is in urgent need to exploit new-type multiferroic materials, and on the other hand, we note that the principle of MTJ allows more magnetic states with different *TMR* values by selecting ferromagnetic layers with more easy-axes [92,127–129]. It implies that the multi-state memory devices with an enhanced capacity of information storage would be achieved through integrating the features of non-collinear magnetization alignments with the ferroelectric polarization switching, such as octonary resistance states in $La_{0.7}Sr_{0.3}MnO_3/BaTiO_3/La_{0.7}Sr_{0.3}MnO_3$ MFTJs, which could be operated by magnetic and electric fields [130]. It is obviously different from the ferroelectric memristors where the multi-states could be obtained by varying the maximum voltage pulse amplitude related to the ferroelectric polarization switching with ferroelectric domain nucleation and growth [131].

Using ferromagnetic manganites as electrodes, one can realize ferroelectric and magnetic fields controlled electric and magnetic properties of multiferroic heterostructures. Owing to the interplay among spin, charge, orbit, and lattice degrees of freedom as well as the interfacial ME coupling effect, these multiferroic heterostructures with new physical properties could be used to design novel functional devices. For example, the MFTJs with four nonvolatile states and even eight resistance states are the new-types of the potential multi-functional devices. Despite all these studies, there are lots of open questions for multiferroic heterostructures and tunneling junctions such as: i) for magnetic field control of electric polarization, how to achieve a giant ME effect at room temperature in low magnetic fields, ii) for electric field control of magnetism, how to experimentally achieve a reversible non-volatile magnetization rotation over a large area of heterostructure without an assistant magnetic fields, and iii) for electric field manipulation on the electronic transport properties, how to simultaneously achieve large *TER* and *TMR* values at room temperature in MFTJs. Thus, further studies are needed for exploring new materials and new technologies to improve the potential applications of the multiferroic heterostructures and tunneling junctions.

Acknowledgments

This work is supported by the National Natural Science Foundation of China and the National Basic Research Program of China (Contract Nos. 2012CB922003 and 2015CB921201).

References

[1] Fiebig M. Revival of the magnetoelectric effect. J Phys D Appl Phys 2005;38:R123–52.
[2] Eerenstein W, Mathur ND, Scott JF. Multiferroic and magnetoelectric materials. Nature 2006;442:759–65.
[3] Prellier W, Singh MP, Murugavel P. The single-phase multiferroic oxides: from bulk to thin film. J Phys Condens Matter 2005;17:R803–32.
[4] Cheong SW, Mostovoy M. Multiferroics a magnetic twist for ferroelectricity. Nat Mater 2007;6:13–20.
[5] Khomskii D. Classifying multiferroics: mechanisms and effects. Physics 2009;2:20.
[6] Tokura Y, Seki S. Multiferroics with spiral spin orders. Adv Mater 2010;22:1554–65.
[7] Catalan G, Scott JF. Physics and applications of bismuth ferrite. Adv Mater 2009;21:2463–85.
[8] Wang J, Neaton JB, Zheng H, Nagarajan V, Ogale SB, Liu B, et al. Epitaxial $BiFeO_3$ multiferroic thin film heterostructures. Science 2003;299:1719–22.
[9] Hu JM, Li Z, Chen LQ, Nan CW. High-density magnetoresistive random access memory operating at ultralow voltage at room temperature. Nat Commun 2011;2:553.
[10] Sando D, Agbelele A, Rahmedov D, Liu J, Rovillain P, Toulouse C, et al. Crafting the magnonic and spintronic response of $BiFeO_3$ films by epitaxial strain. Nat Mater 2013;12:641–6.
[11] Wang KF, Liu JM, Ren ZF. Multiferroicity: the coupling between magnetic and polarization orders. Adv Phys 2009;58:321–448.
[12] Tokunaga M, Akaki M, Ito T, Miyahara S, Miyake A, Kuwahara H, et al. Magnetic control of transverse electric polarization in BiFeO(3). Nat Commun 2015;6:5878.
[13] Hill NA. Why are there so few magnetic ferroelectrics. J Phys Chem B 2000;104:6694–709.
[14] Van Aken BB, Palstra TTM. Influence of magnetic on ferroelectric ordering in $LuMnO_3$. Phys Rev B 2004;69:134113.
[15] Velev JP, Jaswal SS, Tsymbal EY. Multi-ferroic and magnetoelectric materials and interfaces. Phil Trans R Soc A 2011;369:3069–97.
[16] Kimura T. Spiral magnets as magnetoelectrics. Annu Rev Mater Res 2007;37:387–413.
[17] Nan C-W, Bichurin MI, Dong SX, Viehland D, Srinivasan G. Multiferroic magnetoelectric composites: historical perspective, status, and future directions. J Appl Phys 2008;103. 031101.
[18] Srinivasan G. Magnetoelectric composites. Annu Rev Mater Res 2010;40:153–78.
[19] Sun NX, Srinivasan G. Voltage control of magnetism in multiferroic heterostructures and devices. Spin 2012;02:1240004.
[20] Martin LW, Ramesh R. Multiferroic and magnetoelectric heterostructures. Acta Mater 2012;60:2449–70.
[21] Kambale RC, Jeong D-Y, Ryu J. Current status of magnetoelectric composite thin/thick films. Adv Condens Matter Phys 2012;2012:1–15.
[22] Yao XF, Ma J, Lin YH, Nan C-W, Zhang JX. Magnetoelectric coupling across the interface of multiferroic nanocomposites. Sci China Mater 2015;58:143–55.

[23] Liu YK, Yao YP, Dong SN, Jiang T, Yang SW, Li XG. Colossal magnetocapacitance effect in $BiFeO_3/La_{5/8}Ca_{3/8}MnO_3$ epitaxial films. Thin Solid Films 2012;520:5775–8.

[24] Liu YK, Yao YP, Dong SN, Yang SW, Li XG. Effect of magnetic field on ferroelectric properties of $BiFeO_3/La_{5/8}Ca_{3/8}MnO_3$ epitaxial heterostructures. Phys Rev B 2012;86. 075113.

[25] Yang SW, Dong SN, Liu YK, Yao YP, Yin YW, Li XG. Tunable dielectric and ferroelectric properties in heteroepitaxial $PbZr_{0.52}Ti_{0.48}O_3/La_{0.625}Ca_{0.375}MnO_3$ thin films. J Appl Phys 2013;114. 034102.

[26] Feng L, Yang SW, Liu YK, Yin YW, Dong SN, Jiang T, et al. Effects of magnetic electrode on the ferroelectric properties in heteroepitaxial $BiFeO_3/La_{0.625}Ca_{0.375}MnO_3$ thin films. J Appl Phys 2014;115. 094504.

[27] Wu T, Zurbuchen MA, Saha S, Wang RV, Streiffer SK, Mitchell JF. Observation of magnetoelectric effect in epitaxial ferroelectric film/manganite crystal heterostructures. Phys Rev B 2006;73:134416.

[28] Zhu QX, Zheng M, Yang MM, Li XM, Wang Y, Shi X, et al. Effects of ferroelectric-poling-induced strain on magnetic and transport properties of $La_{0.67}Ba_{0.33}MnO_3$ thin films grown on (111)-oriented ferroelectric substrates. Appl Phys Lett 2013;103:132910.

[29] Zhang S, Zhao YG, Li PS, Yang JJ, Rizwan S, Zhang JX, et al. Electric-field control of nonvolatile magnetization in $Co_{40}Fe_{40}B_{20}/Pb(Mg_{1/3}Nb_{2/3})_{0.7}Ti_{0.3}O_3$ structure at room temperature. Phys Rev Lett 2012;108:137203.

[30] Zhang S, Zhao YG, Xiao X, Wu YZ, Rizwan S, Yang LF, et al. Giant electrical modulation of magnetization in $Co_{40}Fe_{40}B_{20}/Pb(Mg_{1/3}Nb_{2/3})_{0.7}Ti_{0.3}O_3(011)$ heterostructure. Sci Rep 2014;4:3727.

[31] Zhu Q-X, Yang M-M, Zheng M, Zheng R-K, Guo L-J, Wang Y, et al. Ultrahigh tunability of room temperature electronic transport and ferromagnetism in dilute magnetic semiconductor and PMN-PT single-crystal-based field effect transistors via electric charge mediation. Adv Funct Mater 2015;25:1111–9.

[32] Ma J, Hu J, Li Z, Nan CW. Recent progress in multiferroic magnetoelectric composites: from bulk to thin films. Adv Mater 2011;23:1062–87.

[33] Geprägs S, Brandlmaier A, Opel M, Gross R, Goennenwein STB. Electric field controlled manipulation of the magnetization in Ni/$BaTiO_3$ hybrid structures. Appl Phys Lett 2010;96:142509.

[34] Asamitsu A, Moritomo Y, Tomioka Y, Arima T, Tokura Y. A structural phase transition induced by an external magnetic field. Nature 1995;373:407–9.

[35] Luo LH, Wang HX, Tang YX, Zhao XY, Feng ZY, Lin D, et al. Ultrahigh transverse strain and piezoelectric behavior in $(1-x)Pb(Mg_{1/3}Nb_{2/3})O_{3-x}PbTiO_3$ crystals. J Appl Phys 2006;99. 024104.

[36] Buzzi M, Chopdekar RV, Hockel JL, Bur A, Wu T, Pilet N, et al. Single domain spin manipulation by electric fields in strain coupled artificial multiferroic nanostructures. Phys Rev Lett 2013;111. 027204.

[37] Ghidini M, Pellicelli R, Prieto JL, Moya X, Soussi J, Briscoe J, et al. Non-volatile electrically-driven repeatable magnetization reversal with no applied magnetic field. Nat Commun 2013;4:1453.

[38] Lou J, Liu M, Reed D, Ren YH, Sun NX. Giant electric field tuning of magnetism in novel multiferroic FeGaB/lead zinc niobate-lead titanate (PZN-PT) Heterostructures. Adv Mater 2009;21:4711–5.

[39] Wu T, Bur A, Zhao P, Mohanchandra KP, Wong K, Wang KL, et al. Giant electric-field-induced reversible and permanent magnetization reorientation on magnetoelectric Ni/(011) $[Pb(Mg_{1/3}Nb_{2/3})O_3]_{(1-x)}-[PbTiO_3]_x$ heterostructure. Appl Phys Lett 2011;98. 012504.

[40] Nan TX, Zhou ZY, Liu M, Yang X, Gao Y, Assaf BA, et al. Quantification of strain and charge co-mediated magnetoelectric coupling on ultra-thin permalloy/PMN-PT interface. Sci Rep 2014;4:3688.

[41] Yang SW, Peng RC, Jiang T, Liu YK, Feng L, Wang JJ, et al. Non-volatile 180 degrees magnetization reversal by an electric field in multiferroic heterostructures. Adv Mater 2014;26:7091–5.

[42] Dong SX, Li J-F, Viehland D. Ultrahigh magnetic field sensitivity in laminates of TERFENOL-D and $Pb(Mg_{1/3}Nb_{2/3})O_3-PbTiO_3$ crystals. Appl Phys Lett 2003;83:2265.

[43] Zhang R, Jiang B, Cao WX. Orientation dependence of piezoelectric properties of single domain $0.67Pb(Mn_{1/3}Nb_{2/3})O_3-0.33PbTiO_3$ crystals. Appl Phys Lett 2003;82:3737.

[44] Mattheis R, Quednau G. Determination of the anisotropy field strength in ultra-thin magnetic films using longitudinal MOKE and a rotating field: the ROTMOKE method. J Magn Magn Mater 1999;205:143–50.

[45] Yang SW, Feng L, Zhang DL, Huang WC, Dong SN, Wang JJ, et al. Magnetically correlated anisotropic resistive switching manipulated by electric field in Co/PMN-PT heterostructures. J Alloys Compd 2015;646:472–6.

[46] Lei N, Devolder T, Agnus G, Aubert P, Daniel L, Kim JV, et al. Strain-controlled magnetic domain wall propagation in hybrid piezoelectric/ferromagnetic structures. Nat Commun 2013;4:1378.

[47] Cherifi RO, Ivanovskaya V, Phillips LC, Zobelli A, Infante IC, Jacquet E, et al. Electric-field control of magnetic order above room temperature. Nat Mater 2014;13:345–51.

[48] Zhou ZY, Howe BM, Liu M, Nan TX, Chen X, Mahalingam K, et al. Interfacial charge-mediated non-volatile magnetoelectric coupling in $Co_{0.3}Fe_{0.7}/Ba_{0.6}Sr_{0.4}TiO_3/Nb:SrTiO_3$ multiferroic heterostructures. Sci Rep 2015;5:7740.

[49] Maruyama T, Shiota Y, Nozaki T, Ohta K, Toda N, Mizuguchi M, et al. Large voltage-induced magnetic anisotropy change in a few atomic layers of iron. Nat Nanotechnol 2009;4:158–61.

[50] Zhou Z, Nan TX, Gao Y, Yang X, Beguhn S, Li M, et al. Quantifying thickness-dependent charge mediated magnetoelectric coupling in magnetic/dielectric thin film heterostructures. Appl Phys Lett 2013;103:232906.

[51] Mardana A, Ducharme S, Adenwalla S. Ferroelectric control of magnetic anisotropy. Nano Lett 2011;11:3862–7.

[52] Yi D, Liu J, Okamoto S, Jagannatha S, Chen Y-C, Yu P, et al. Tuning the competition between ferromagnetism and antiferromagnetism in a half-doped manganite through magnetoelectric coupling. Phys Rev Lett 2013;111:127601.

[53] Kawano H. Canted antiferromagnetism in an insulating lightly doped $La_{1-x}Sr_xMnO_3$ with $x < 0.17$. Phys Rev B 1996;53:2202–5.

[54] Solovyev IV, Terakura K. Spin canting in three-dimensional perovskite manganites. Phys Rev B 2001;63:174425.

[55] Molegraaf HJA, Hoffman J, Vaz CAF, Gariglio S, van der Marel D, Ahn CH, et al. Magnetoelectric effects in complex oxides with competing ground states. Adv Mater 2009;21:3470–4.

[56] Vaz CAF, Hoffman J, Segal Y, Reiner JW, Grober RD, Zhang Z, et al. Origin of the magnetoelectric coupling effect in $Pb(Zr_{0.2}Ti_{0.8})O_3/La_{0.8}Sr_{0.2}MnO_3$ multiferroic heterostructures. Phys Rev Lett 2010;104:127202.

[57] Spurgeon Steven R, S JD, Kepaptsoglou Despoina Maria, Balachandran Prasanna V, Nejati Siamak, Karthik J, et al. Thickness-dependent crossover from charge- to strain-mediated magnetoelectric coupling in ferromagnetic/piezoelectric oxide heterostructures. ACS Nano 2014;8:894–903.

[58] Chang HJ, Kalinin SV, Morozovska AN, Huijben M, Chu YH, Yu P, et al. Atomically resolved mapping of polarization and electric fields across ferroelectric/oxide interfaces by Z-contrast imaging. Adv Mater 2011;23:2474–9.

[59] Kim Y-M, Morozovska A, Eliseev E, Oxley MP, Mishra R, Selbach SM, et al. Direct observation of ferroelectric field effect and vacancy controlled screening at the $BiFeO_3/La_xSr_{1-x}MnO_3$ interface. Nat Mater 2014;13:1019–25.

[60] Chen HH, Qiao Q, Marshall MS, Georgescu AB, Gulec A, Phillips PJ, et al. Reversible modulation of orbital occupations via an interface-induced polar state in metallic manganites. Nano Lett 2014;14:4965–70.

[61] Samet L, Imhoff D, Maurice JL, Contour JP, Gloter A, Manoubi T, et al. EELS study of interfaces in magnetoresistive LSMO/STO/LSMO tunnel junctions. Eur Phys J B 2003;34:179–92.

[62] Schmid HK, Mader W. Oxidation states of Mn and Fe in various compound oxide systems. Micron 2006;37:426–32.

[63] Liu M, Hoffman J, Wang J, Zhang JX, Nelson-Cheeseman B, Bhattacharya A. Non-volatile ferroelastic switching of the Verwey transition and resistivity of epitaxial Fe_3O_4/PMN-PT (011). Sci Rep 1876;2013:3.

[64] Jiang L, Seok Choi W, Jeen H, Egami T, Nyung Lee H. Strongly coupled phase transition in ferroelectric/correlated electron oxide heterostructures. Appl Phys Lett 2012;101. 042902.

[65] Jiang T, Yang SW, Liu YK, Yin YW, Dong SN, Zhao WB, et al. Coaction and distinguishment of converse piezoelectric and field effects in $La_{0.7}Ca_{0.3}MnO_3/SrTiO_3/0.68Pb(Mg_{1/3}Nb_{2/3})O_3$-$0.32PbTiO_3$ heterostructures. Appl Phys Lett 2013;103. 053504.

[66] Choi T, Lee S, Choi YJ, Kiryukhin V, Cheong S-W. Switchable ferroelectric diode and photovoltaic effect in $BiFeO_3$. Science 2009;324:63–6.

[67] Yao YP, Liu YK, Dong SN, Yin YW, Yang SW, Li XG. Multi-state resistive switching memory with secure information storage in Au/$BiFe_{0.95}Mn_{0.05}O_3/La_{5/8}Ca_{3/8}MnO_3$ heterostructure. Appl Phys Lett 2012;100:193504.

[68] Jiang AQ, Wang C, Jin KJ, Liu XB, Scott JF, Hwang CS, et al. A resistive memory in semiconducting $BiFeO_3$ thin-film capacitors. Adv Mater 2011;23:1277–81.

[69] You TG, Shuai Y, Luo WB, Du N, Bürger D, Skorupa I, et al. Exploiting memristive $BiFeO_3$ bilayer structures for compact sequential logics. Adv Funct Mater 2014;24:3357–65.

[70] Chen X, Jia CH, Chen YH, Yang G, Zhang WF. Ferroelectric memristive effect in BaTiO3 epitaxial thin films. J Phys D Appl Phys 2014;47:365102.

[71] Tsymbal EY, Kohlstedt H. Tunneling across a ferroelectric. Science 2006;313:181–3.

[72] Esaki L, Laibowitz RB, Stiles PJ. Nonvolatile Schottky diode with barrier height controlled by ferroelectric polarization. IBM Tech Discl Bull 1971;13:2161.

[73] Tenne DA, Bruchhausen A, Lanzillotti-Kimura ND, Fainstein A, Katiyar RS, Cantarero A, et al. Probing nanoscale ferroelectricity by ultraviolet Raman spectroscopy. Science 2006;313:1614–6.

[74] Fong DD, Stephenson GB, Streiffer SK, Eastman JA, Auciello O, Fuoss PH, et al. Ferroelectricity in ultrathin perovskite films. Science 2004;304:1650–3.

[75] Lichtensteiger C, Triscone J-M, Junquera J, Ghosez P. Ferroelectricity and tetragonality in ultrathin $PbTiO_3$ films. Phys Rev Lett 2005;94. 047603.

[76] Li JY, Li J-F, Yu Q, Chen QN, Xie SH. Strain-based scanning probe microscopies for functional materials, biological structures, and electrochemical systems. J Materiomics 2015;1:3–21.

[77] Garcia V, Fusil S, Bouzehouane K, Enouz-Vedrenne S, Mathur ND, Barthelemy A, et al. Giant tunnel electroresistance for non-destructive readout of ferroelectric states. Nature 2009;460:81–4.

[78] Gruverman A, Wu D, Lu H, Wang Y, Jang HW, Folkman CM, et al. Tunneling electroresistance effect in ferroelectric tunnel junctions at the nanoscale. Nano Lett 2009;9:3539.

[79] Ou X, Xu B, Gong CJ, Lan XX, Yin QN, Xia YD, et al. Continuously-tuned tunneling behaviors of ferroelectric tunnel junctions based on $BaTiO_3/La_{0.67}Sr_{0.33}MnO_3$ heterostructure. AIP Adv 2014;4. 057106.

[80] Zp Li, Guo X, Lu HB, Zhang ZL, Song DS, Cheng SB, et al. An epitaxial ferroelectric tunnel junction on silicon. Adv Mater 2014;26:7185–9.

[81] Maksymovych P, Jesse S, Yu P, Ramesh R, Baddorf AP, Kalinin SV. Polarization control of electron tunneling into ferroelectric surfaces. Science 2009;324:1421–5.

[82] Crassous A, Garcia V, Bouzehouane K, Fusil S, Vlooswijk AHG, Rispens G, et al. Giant tunnel electroresistance with $PbTiO_3$ ferroelectric tunnel barriers. Appl Phys Lett 2010;96. 042901.

[83] Jiang L, Choi WS, Jeen H, Dong S, Kim Y, Han M-G, et al. Tunneling electroresistance induced by interfacial phase transitions in ultrathin oxide heterostructures. Nano Lett 2013;13:5837–43.

[84] Chanthbouala A, Crassous A, Garcia V, Bouzehouane K, Fusil S, Moya X, et al. Solid-state memories based on ferroelectric tunnel junctions. Nat Nanotechnol 2011;7:101–4.

[85] Wen Z, Li C, Wu D, Li AD, Ming NB. Ferroelectric-field-effect-enhanced electroresistance in metal-ferroelectric-semiconductor tunnel junctions. Nat Mater 2013;12:617–21.

[86] Soni R, Petraru A, Meuffels P, Vavra O, Ziegler M, Kim SK, et al. Giant electrode effect on tunnelling electroresistance in ferroelectric tunnel junctions. Nat Commun 2014;5:5414.

[87] Moodera JS, Kinder LR, Wong TM, Meservey R. Large magnetoresistance at room temperature in ferromagnetic thin film tunnel junctions. Phys Rev Lett 1995;74:3273–6.

[88] Parkin SS, Kaiser C, Panchula A, Rice PM, Hughes B, Samant M, et al. Giant tunnelling magnetoresistance at room temperature with MgO (100) tunnel barriers. Nat Mater 2004;3:862–7.

[89] Jia Z, Misra RDK. Magnetic sensors for data storage: perspective and future outlook. Mater Tech 2011;26:191–9.

[90] Miao G-X, Münzenberg M, Moodera JS. Tunneling path toward spintronics. Rep Prog Phys 2011;74. 036501.

[91] Julliere M. Tunneling between ferromagnetic films. Phys Lett A 1975;54:225–6.

[92] Cuellar FA, Liu YH, Salafranca J, Nemes N, Iborra E, Sanchez-Santolino G, et al. Reversible electric-field control of magnetization at oxide interfaces. Nat Commun 2014;5:4215.

[93] Zhuravlev MY, Jaswal SS, Tsymbal EY, Sabirianov RF. Ferroelectric switch for spin injection. Appl Phys Lett 2005;87:222114.

[94] Zhuravlev MY, Maekawa S, Tsymbal EY. Effect of spin-dependent screening on tunneling electroresistance and tunneling magnetoresistance in multiferroic tunnel junctions. Phys Rev B 2010;81:104419.

[95] Tsymbal EY, Gruverman A, Garcia V, Bibes M, Barthélémy A. Ferroelectric and multiferroic tunnel junctions. MRS Bull 2012;37:138–43.

[96] Garcia V, Bibes M. Ferroelectric tunnel junctions for information storage and processing. Nat Commun 2014;5:4289.

[97] Velev JP, Duan CG, Burton JD, Smogunov A, Niranjan MK, Tosatti E, et al. Magnetic tunnel junctions with ferroelectric barriers prediction of four resistance states from first principles. Nano Lett 2009;9:427–32.

[98] Garcia V, Bibes M, Bocher L, Valencia S, Kronast F, Crassous A, et al. Ferroelectric control of spin polarization. Science 2010;327:1106–10.

[99] Duan C-G, Jaswal SS, Tsymbal EY. Predicted magnetoelectric effect in Fe/$BaTiO_3$ multilayers: ferroelectric control of magnetism. Phys Rev Lett 2006;97. 047201.

[100] Fechner M, Maznichenko I, Ostanin S, Ernst A, Henk J, Bruno P, et al. Magnetic phase transition in two-phase multiferroics predicted from first principles. Phys Rev B 2008;78:212406.

[101] Valencia S, Crassous A, Bocher L, Garcia V, Moya X, Cherifi RO, et al. Interface-induced room-temperature multiferroicity in $BaTiO_3$. Nat Mater 2011;10:753–8.

[102] Bocher L, Gloter A, Crassous A, Garcia V, March K, Zobelli A, et al. Atomic and electronic structure of the $BaTiO_3$/Fe interface in multiferroic tunnel junctions. Nano Lett 2012;12:376–82.

[103] Radaelli G, Petti D, Plekhanov E, Fina I, Torelli P, Salles BR, et al. Electric control of magnetism at the Fe/$BaTiO_3$ interface. Nat Commun 2014;5:3404.

[104] Pantel D, Goetze S, Hesse D, Alexe M. Reversible electrical switching of spin polarization in multiferroic tunnel junctions. Nat Mater 2012;11:289–93.

[105] Gajek M, Bibes M, Fusil S, Bouzehouane K, Fontcuberta J, Barthelemy A, et al. Tunnel junctions with multiferroic barriers. Nat Mater 2007;6:296–302.

[106] Wang F, Leppävuori S. Properties of epitaxial ferroelectric $PbZr_{0.56}Ti_{0.44}O_3$ heterostructures with $La_{0.5}Sr_{0.5}O_3$ metallic oxide electrodes. J Appl Phys 1997;82:1293.

[107] Mathews S, Ramesh R, Venkatesan T, Benedetto J. Ferroelectric field effect transistor based on epitaxial perovskite heterostructures. Science 1997;276:238–40.

[108] Hong X, Posadas A, Lin A, Ahn CH. Ferroelectric-field-induced tuning of magnetism in the colossal magnetoresistive oxide $La_{1-x}Sr_xMnO_3$. Phys Rev B 2003;68:134415.
[109] Pantel D, Goetze S, Hesse D, Alexe M. Room-temperature ferroelectric resistive switching in ultrathin $Pb(Zr_{0.2}T_{i0.8})O_3$ films. ACS Nano 2011;5:6032–8.
[110] Hambe M, Petraru A, Pertsev NA, Munroe P, Nagarajan V, Kohlstedt H. Crossing an interface: ferroelectric control of tunnel currents in magnetic complex oxide heterostructures. Adv Funct Mater 2010;20:2436–41.
[111] Zhao T, Scholl A, Zavaliche F, Lee K, Barry M, Doran A, et al. Electrical control of antiferromagnetic domains in multiferroic $BiFeO_3$ films at room temperature. Nat Mater 2006;5:823–9.
[112] Wu SM, Cybart SA, Yi D, Parker JM, Ramesh R, Dynes RC. Full electric control of exchange bias. Phys Rev Lett 2013;110. 067202.
[113] Liu YK, Yin YW, Dong SN, Yang SW, Jiang T, Li XG. Coexistence of four resistance states and exchange bias in $La_{0.6}Sr_{0.4}MnO_3/BiFeO_3/La_{0.6}Sr_{0.4}MnO_3$ multiferroic tunnel junction. Appl Phys Lett 2014;104. 043507.
[114] Yin YW, Raju M, Hu WJ, Weng XJ, Zou K, Zhu J, et al. Multiferroic tunnel junctions. Front Phys 2012;7:380–5.
[115] Yin YW, Burton JD, Kim Y-M, Borisevich AY, Pennycook SJ, Yang SM, et al. Enhanced tunnelling electroresistance effect due to a ferroelectrically induced phase transition at a magnetic complex oxide interface. Nat Mater 2013;12:397–402.
[116] Burton JD, Tsymbal EY. Giant tunneling electroresistance effect driven by an electrically controlled spin valve at a complex oxide interface. Phys Rev Lett 2011;106:157203.
[117] Ramirez AP. Colossal magnetoresistance. J Phys Condens Matter 1997;9:8171–99.
[118] Burton JD, Tsymbal EY. Prediction of electrically induced magnetic reconstruction at the manganite/ferroelectric interface. Phys Rev B 2009;80:174406.
[119] Yin YW, Raju M, Hu WJ, Weng XJ, Li XG, Li Q. Coexistence of tunneling magnetoresistance and electroresistance at room temperature in $La_{0.7}Sr_{0.3}MnO_3$/(Ba, Sr)TiO_3/$La_{0.7}Sr_{0.3}MnO_3$ multiferroic tunnel junctions. J Appl Phys 2011;109. 07D915.
[120] Glazman LI, Matveev KA. Inelastic tunneling across thin amorphous films. Sov Phys JETP 1988;67:1276–82.
[121] Hu JM, Yang TN, Wang JJ, Huang HB, Zhang JX, Chen LQ, et al. Purely electric-field-driven perpendicular magnetization reversal. Nano Lett 2015;15:616–22.
[122] Heron J, Trassin M, Ashraf K, Gajek M, He Q, Yang S, et al. Electric-field-induced magnetization reversal in a ferromagnet-multiferroic heterostructure. Phys Rev Lett 2011;107:217202.
[123] Skumryev V, Laukhin V, Fina I, Martí X, Sánchez F, Gospodinov M, et al. Magnetization reversal by electric-field decoupling of magnetic and ferroelectric domain walls in multiferroic-based heterostructures. Phys Rev Lett 2011;106. 057206.
[124] Zhu WJ, Xiao D, Liu YW, Gong SJ, Duan C-G. Picosecond electric field pulse induced coherent magnetic switching in MgO/FePt/Pt(001)-based tunnel junctions: a multiscale study. Sci Rep 2014;4:4117.
[125] Jin HZ, Zhu J. Size effect and fatigue mechanism in ferroelectric thin films. J Appl Phys 2002;92:4594.
[126] Yang F, Tang MH, Ye Z, Zhou YC, Zheng XJ, Tang JX, et al. Eight logic states of tunneling magnetoelectroresistance in multiferroic tunnel junctions. J Appl Phys 2007;102. 044504.
[127] Yoo T, Khym S, Lee H, Lee S, Lee S, Liu XY, et al. Tunneling magnetoresistance from non-collinear alignment of magnetization in Fe/GaAlAs/GaMnAs magnetic tunnel junctions. Appl Phys Lett 2013;102:212404.
[128] Yoo T, Lee S, Liu XY, Furdyna JK, Lee DU, Kim EK. Decimal tunneling magnetoresistance states in Fe/GaAlAs/GaMnAs magnetic tunnel junction. IEEE Trans Magn 2014;50:4401104.
[129] Fang YY, Dumas RK, Nguyen TNA, Mohseni SM, Chung S, Miller CW, et al. A nonvolatile spintronic memory element with a continuum of resistance states. Adv Funct Mater 2013;23:1919–22.
[130] Yin YW, Huang WC, Liu YK, Yang SW, Dong SN, Tao J, et al. Octonary resistance states in La0.7Sr0.3MnO3/BaTiO3/La0.7Sr0.3MnO3 multiferroic tunnel junctions. Adv Electron Mater 2015 (Accepted).
[131] Chanthbouala A, Garcia V, Cherifi R, Bouzehouane K, Fusil S, Moya X, et al. A ferroelectric memristor. Nat Mater 2012;11:860–4.

Weichuan HUANG, University of Science and Technology of China. Email: wchhuang@mail.ustc.edu.cn. **Weichuan HUANG** is a PhD student of condensed matter physics of Hefei National Laboratory for Physical Sciences at Microscale, University of Science and Technology of China, Hefei, China. He obtained his Bachelor's Degree in 2013 from the Institute for Advanced Materials, South China Academy of Advanced Photonics Engineering, South China Normal University, Guangzhou, China. His research interests focus on the fabrication and properties of multiferroic tunneling junctions.

Shengwei YANG, University of Science and Technology of China. Email: yangsw94@mail.ustc.edu.cn. **Shengwei YANG** is a PhD of condensed matter physics. He graduated from Department of Physics, University of Science and Technology of China, where he received his Bachelor and Doctor Degrees in 2010 and 2015, respectively. His research interests focus on the fabrication and properties of multiferroic heterostructures.

Professor Xiaoguang LI, University of Science and Technology of China. Email: lixg@ustc.edu.cn. Dr. **Xiaoguang LI** is a professor of materials physics, Hefei National Laboratory for Physical Sciences at Microscale, Department of Physics, University of Science and Technology of China. He received PhD in 1989 from the Institute of Solid State Physics, Chinese Academy of Sciences. He worked in University of Tokyo as a JSPS Research Fellow from 1993 to 1994. He became a faculty member in the University of Science and Technology of China as a full professor in 1993. Research interests include synthesis, microstructure, physical properties and prototype of the related devices for transitional metal oxides.